Synthesis of High Metal Loading Single Atom Catalysts and Exploration of the Active Center Structure

Kaiying Wang,[a] Xiaofeng Wang,[b] Xinhua Liang*,[a]

[a] K. Wang, Department of Chemical and Biochemical Engineering, Missouri University of Science and Technology, Rolla, MO 65409, United States
[b] Prof. X. Wang, College of Environmental Science and Engineering, Dalian Maritime University, Dalian 116026, P.R. China
[a] Prof. X. Liang, Department of Chemical and Biochemical Engineering, Missouri University of Science and Technology, Rolla, MO 65409, United States, Email: liangxin@mst.edu

Abstract

Single-atom catalysts (SACs) have been rising recently as a new frontier in the catalysis field. Due to maximum atom utilization efficiency and tunable electronic structures, SACs exhibit highly distinctive catalytic performance from bulk counterparts. SACs with high metal loading will facilitate practical applications. To that end, this review focuses on recent strategies to maximize metal loading. An appropriate substrate, mainly heteroatom-doped carbon materials, is the key to avoiding aggregation or sintering during synthetic procedures. The coordination site construction and spatial confinement strategies are adopted to prepare SACs with high metal loading. Advanced characterization techniques with atomic resolution are indispensable for identification of the exact structure of SACs. This is true, especially for the applications and challenges in developing *in situ*/operando characterization techniques at the atomic level, which are discussed in this review. Moreover, it is fundamentally necessary to investigate the active center structure, which facilitates any design of efficient SACs that can maximize single-atom catalytic activity. Furthermore, this review highlights challenges and prospects for development of SACs.

1. Introduction

Supported metal catalysts, especially noble metals, are the most widely used in the heterogeneous catalysis field. However, their scarcity and high cost impede the widespread implementation of noble metal catalysts.[1] Thus, it is essential that the usage of noble metals is reduced and that their high catalytic activity is simultaneously retained. An effective way to maximize atom utilization is to reduce the particle size to atomically dispersed atoms.[2-15] Single-atom catalysts (SACs) have been recently rising as a new frontier in the catalysis field. The discovery of SACs can be traced

back for decades. Thomas et al. grafted titanium (Ti) species onto the inner walls of mesoporous silica MCM-41 to obtain well-separated Ti active sites in 1995;[16] Ti species may be individually dispersed, since no obvious nanoparticles (NPs) were detected. In 2003, Schrock et al. found nitrogen could be reduced to ammonia under mild conditions at a single molybdenum (Mo) center that cycled from Mo(III) through Mo(VI) states.[17] In the same year, Flytzani-Stephanopoulos et al. conducted a water-gas shifting (WGS) reaction using NaCN solution leached gold (Au) and platinum (Pt) catalysts.[18] They found that nonmetallic Au or Pt species that were strongly associated with surface cerium-oxygen groups were responsible for the activity, while NPs did not participate in the reaction. Similar results were observed by Xu et al., where isolated Au^{3+} was the active center for the hydrogenation of 1,3-butadiene.[19] All of these works suggested that single atoms may be the active center, but systematic characterizations of these catalysts were impossible to do because of the limited characterization techniques available at that time. Fortunately, the rapid development of advanced characterization techniques has allowed full characterization of SACs to come true. Zhang et al. comprehensively investigated Pt_1/FeO_x SACs with atomic-resolution aberration-corrected high-angle-annular-dark-field scanning transmission electron microscopy (AC-HAADF-STEM), X-ray absorption spectroscopy (XAS), and *in situ* diffuse reflectance infrared Fourier transform spectroscopy (DRIFTS), thereby sparking enthusiasm for the development of well-defined catalysts.[20]

To improve the overall activity of SACs, the number of active sites should be increased (e.g., through increased loading or improved catalyst structure) to expose more active sites per gram.[21-23] The metal loadings of previously reported SACs usually were kept lower than 1 wt.% to ensure atomic dispersion.[24-26] The low metal loadings severely limited the overall performance, hindering their potential applications, especially at the industrial level.[27] Although some SACs may have some orders of magnitude higher activity than their NP counterparts, based on turnover frequency (TOF), the reaction rate per overall catalyst mass of SACs is at least one order of magnitude lower than that of supported NPs.[28] In most cases, the space-time yield of SACs is still lower than that of NPs, due to the low metal loadings of SACs.[29] Moreover, dense atomic dispersion could result in some synergistic effect between the neighboring single atoms.[23, 30-31] However, it is a great challenge to prepare SACs with high metal loading, since the high surface energy makes the atomically dispersed metal atoms aggregate easily.[32] Several review papers have summarized various synthesis methods,[33-35] including the wet-chemistry method,[20] atomic

layer deposition (ALD) method,[36-37] anti-Ostwald ripening,[38-39] ball milling,[40] and mass selection with soft-landing.[41] None of these reviews focus on the preparation of high metal loading SACs. In this regard, it is highly desirable to propose synthesis strategies for SACs with metal loading higher than 5 wt.%, where suitable substrates play critical roles. Heteroatom-doped carbon materials with sufficient anchoring sites will be highlighted. Besides, effective approaches, such as coordination of site construction and spatial confinement strategies, will be used to prepare SACs with high metal loading.

The use of advanced characterization techniques is essential for confirming the structures of SACs, and a few review papers have been published about characterizations of SACs.[42-45] However, *in situ* characterization of SACs are rarely mentioned. In this review, *in situ* characterization techniques will be highlighted. Owing to *in situ* characterization techniques, the dynamic progress under real reaction conditions can be captured. The transformation of the geometric structure, as well as the electronic environment of the catalytic sites, can also be recorded. Besides, the limitations and challenges facing the development of characterization techniques will be discussed.

SACs have been used in various heterogeneous catalytic applications,[28, 33-35, 46-53] including carbon monoxide (CO) oxidation,[54-61] selective hydrogenation,[26, 62-66] WGS reaction,[67-71] and electrocatalysis.[25, 72-89] It is important to understand the real active centers, that guide the design of catalysts from a trial-and-error practice into a reasonable design. SACs are ideal models for active centers analysis, compared to their NP counterparts. NPs usually contain sites at terraces, edges, and corners, which complicate the catalytic process.[90] In this review, strategies for fabricating optical active centers will be summarized, including pretreatment of synthesized SACs, preparation of dimers, adjustment of coordination environments and metal-support interactions, and synthesis of single-atom alloy (SAA). With a suitable active center, the obtained SACs can maximize the intrinsic activity of each active site, improving the catalyst activity.

In this review, we offer an overview of recent research findings on synthesis strategies for SACs with high metal loading, *in situ* characterization of SACs, and analysis of the active center of SACs. In addition, the future outlook and expected improvements will be discussed in the last section.

2. Synthesis Strategies of High Metal Loading SACs

Despite the excellent activity of SACs, metal loading is usually kept low to avoid sintering,[10, 91-92] which seriously curbs comprehensive catalytic performance and limits practical utilizations. High loading SACs (> 5 wt.%) are still rarely reported. Basically, the competition between atomic dispersion and aggregation into NPs is, in essence, competition between metal-support interactions and metal-metal bonds of NPs.[93] Thus, a suitable substrate, which can offer strong metal-support interactions, is essential for the synthesis of high metal loading SACs. Besides, smart strategies are required to prepare high metal loading SACs.[27, 94-97] Usually, atoms like nitrogen (N)[98] and sulfur (S)[99] that contain lone pairs of electrons, have robust coordination ability with metal atoms, serving as coordination sites to stabilize single metal atoms. Therefore, constructing coordination atoms, as anchoring sites, is an effective approach to synthesizing high metal loading SACs. The spatial confinement strategy is another effective approach. Porous materials, like metal-organic frameworks (MOFs),[100-102] can encapsulate the metal precursors to prevent migration and aggregation. This review will discuss high metal loading SACs, prepared with coordination site construction and spatial confinement strategies. Table 1 summarizes SACs with high metal loadings (> 5 wt.%).

Table 1. Summary of recently reported SACs with high metal loadings (> 5 wt.%)

Metal	Materials	Loading[wt.%]	Metal	Materials	Loading[wt.%]
Pt	Pt/ZTC[99]	5.0	Fe	Fe-SACs[123]	7.7 ± 1.3
Pt	Pt/MoS_2[78]	7.5	Fe	FeSAs/PTF[113]	8.3
Pt	Pt/meso_S-C[136]	10.0	Fe	$FeN_x/g\text{-}C_3N_4$[91]	18.2
Pt	PtSA-MNSs[74]	12.0	Fe	Fe-NC SACs[110]	8.9
Pt	Pt_1/ATO[61]	8.0	Co	NiSA-N-CNT[119]	7.6
Ir	Ir/meso_S-C[136]	10.0	Co	Co-NC SACs[110]	12.1
Ir	$Ir(CO)_2/rGA$[141]	14.8	Co	SCoNC[126]	15.3
Pd	Pd/meso_S-C[136]	5.0	Co	CoSAs/PTF[112]	5.15
Rh	Rh/meso_S-C[136]	5.0	Ni	Ni-SACs[116]	5.3
Ru	Ru_1/LDH[140]	7.0	Ni	NiSA-N-CNT[118]	20.3
Cu	Cu-N-C[111]	20.9	Ni	NiSA-N-CNT[119]	19 ± 3
Cu	Cu/G[109]	5.4	Ni	Ni SA/NCNTs[124]	6.63

Mo	SA-Mo/NPC[105]	9.54	Ni	Ni SACs[125]	5.44
Mo	Mo-NC SACs[110]	7.8	Zn	Zn–N–C[114]	9.33

2.1. N-contained substrates

The presence of electronegative "N" in the substrates provides suitable sites to anchor the metal species through the coordination of an available "free" lone pair.[103] Inspired by this consideration, substrates with a high content of N are designed to prepare high metal loading SACs. N-contained carbon-based materials, with diversified structures, have been widely used to anchor metal atoms and avoid aggregation. N-contained carbon-based substrates can be obtained directly by pyrolysis N-contained precursors,[104-108] or can be generated *in situ* by pyrolysis of graphitic carbon nitride ($g\text{-}C_3N_4$),[109-111] or porous polymeric materials like covalent triazine frameworks (CTFs),[112-113] and MOFs.[100-102]

2.1.1. Pyrolysis of N-contained precursors

A simple approach to introduce N is to mix the metal precursors with N-contained precursors, which can be chelated with the metal atoms to stabilize the obtained $M\text{-}N_x$ during pyrolysis.[114] For example, Xin et al. mixed ammonium molybdate ($(NH_4)_6Mo_7O_{24}$) with glucose and hydroxylamine hydrochloride to prepare Mo SACs.[105] The mixture was stirred at 70 °C for 16 h to evaporate water and ethanol. The precursor powder was placed in a crucible, heated from room temperature to 650 °C in an argon (Ar) atmosphere, and kept for 4 h, yielding Mo SACs with metal loading of 9.54 wt.%. As shown in Figure 1a, the 3D interconnected carbon frameworks etched by NH_3 produced from the decomposition of the hydroxylamine hydrochloride provided sufficient sites for anchoring the Mo atoms. In the electrocatalytic N_2 reduction reaction, Mo-N sites were considered as the active centers, which corresponded with a previous report.[115] The Mo SACs with 9.54 wt.% of Mo exhibited the best performance, while catalysts with a higher content of Mo had worse results, due to the formation of Mo nanoclusters. Dicyandiamide (DCD), with 66.67 wt.% nitrogen, was another commonly used N source. Baek et al. fabricated Cu SACs with 20.9 wt.% loading by mixing a nitrogen-free Cu MOF ($Cu(BTC)(H_2O)_3$) with DCD.[111] The mixture went through thermal treatment at 800 °C in an Ar atmosphere for 3 h. Then, oxygen saturated 5% hydrochloric acid (HCl) was used to leach the unreacted residues to obtain Cu SACs. Cu atoms

were firmly coordinated with N atoms from DCD, preventing Cu single atoms from "Ostwald ripening".

Following the same strategy, a large-scale preparation of transition metal M-SACs was synthesized by complexing metal precursors with 1,10-phenanthroline, as shown in Figure 1b. The obtained metal complexes were adsorbed onto carbon black, followed by pyrolysis of the surface-modified carbons in an Ar atmosphere at 600 °C for 2 h.[116] The metal loading can be up to 5.3 wt.% for Ni-SACs. More importantly, 1.6 kg of Ni-SACs was obtained in a single synthesis batch with high metal loading. During the preparation, the "porphyrin-like" MN_4 sites were tightly anchored on a carbon black surface, preventing the formation of metal clusters or NPs. Besides, the direct use of a conductive carbon circumvented high temperature pyrolysis. This synthesis strategy paved the way for the large-scale preparation of SACs with high metal loadings.

The metal-N coordination between the metal precursors and N-contained precursors helps stabilize the dispersion of single atoms during the pyrolysis process. N can be doped to the carbon materials by decomposing N-contained precursors, avoiding the use of gaseous ammonia.[117] Such thermal treatment should be conducted in an inert gas atmosphere.

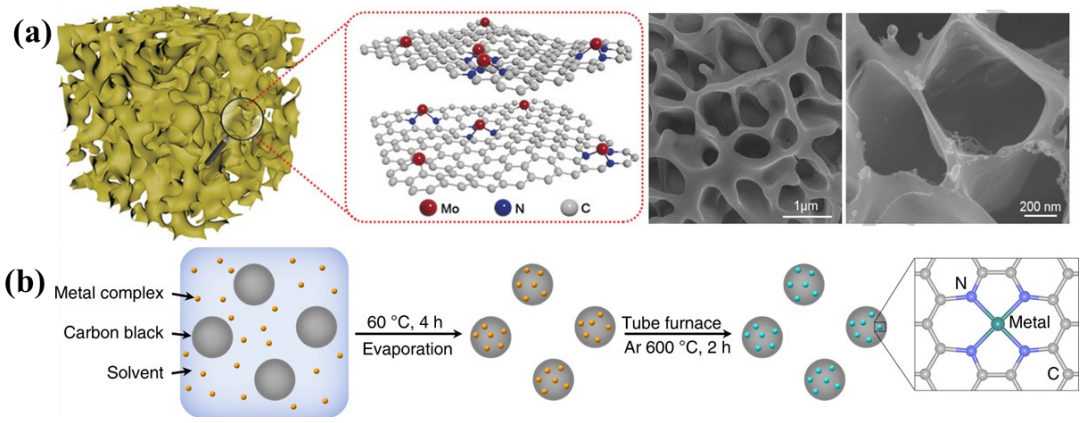

Figure 1. (a) Description of Mo SACs and a corresponding atomic structure model,[105] reprinted with permission from ref [105], Copyright 2019 John Wiley and Sons. (b) General synthesis procedure for transition metal SACs,[116] reprinted with permission from ref [116], Copyright 2019 Nature Publishing Group.

2.1.2. Pyrolysis of *in situ* generated g-C_3N_4

g-C_3N_4 plays a critical role in the synthesis of high metal loading SACs because of its high N content (~60 wt.%). This material can be generated *in situ* through thermal polymerization of different N-rich precursors, such as melamine, urea, DCD, and thiourea. For instance, a multi-step pyrolysis process was used to prepare a class of SACs on N-doped carbon nanotubes (CNTs). The Ni loadings of the Ni SACs can be as high as 20 wt.%.[118-119] In a typical synthesis process, $Ni(acac)_2$ was first atomically dispersed in DCD due to the weak van der Waal's force, and the mixture was then stirred for 10 h before drying at 70 °C. In the multi-step pyrolysis process, shown in Figure 2a, Ni-g-C_3N_4 was formed *in situ* by condensation of melem at 650 °C.[118] The formation of Ni-g-C_3N_4 impeded the sintering of Ni atoms by confining them in the cavity of g-C_3N_4.[120-121] Finally, Ni SACs, with Ni-N_4 structure, were obtained from 700 to 900 °C. The dynamic process of Ni SACs formation was recorded through *in situ* AC-STEM-HAADF. The growth mechanism of Ni SACs was different from that of CNTs.[122] The obtained Ni SACs were used in electrochemical reduction of CO_2, showing two orders of magnitude higher activity than that of CNTs supported Ni NPs. It is worth mentioning that this method can also be used to synthesize bimetallic SACs, such as NiCo, CoFe, and NiPt SACs.

Based on the above-mentioned research, the same group synthesized Fe SACs on N-doped graphene with a Fe loading of ~7.7±1.3 wt.%.[123] Hemin porcine (HP) and DCD were the preferred precursors, which were grounded under the addition of ethanol. The mixture underwent a thermal treatment in an Ar atmosphere. The synthesis process is schematically shown in Figure 2b. The high N content provided sufficient anchoring sites for the Fe single atoms, yielding high Fe loading. AC-STEM confirmed that Fe SACs were distributed across the graphene structure homogeneously. The cathode made by the obtained Fe SACs exhibited superior stability, showing a novel way to design practical catalysts to substitute for commercial Pt/C catalysts.

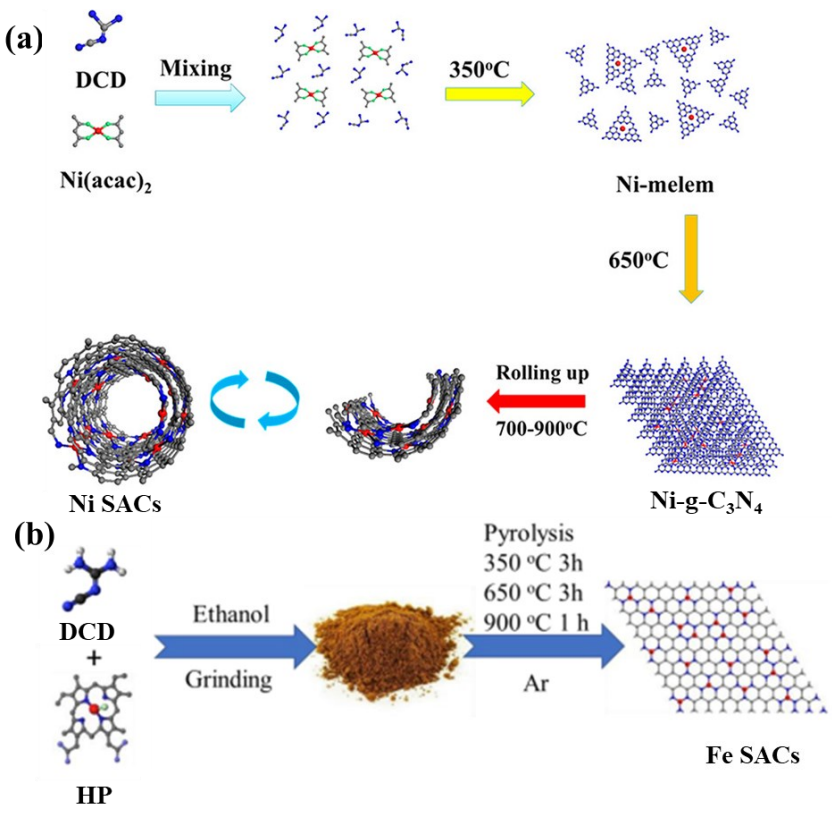

Figure 2. (a) Formation of NiSA-N-CNT,[118] reprinted with permission from ref [118], Copyright 2018 American Chemical Society. (b) Schematic illustration of the one-pot synthesis of 2D Fe single iron atom doped graphene (FeSA-G),[123] reprinted with permission from ref [123], Copyright 2019 John Wiley and Sons.

Following the same strategy, Cu SACs with Cu loading of 5.4 wt.% on graphene[109] and Fe SACs with a high metal loading of 18.2 wt.% were prepared,[91] as shown in Figures 3a and 3b. More important, a general strategy for fabricating a wide range of metal SACs with metal loadings up to 12.1 wt.% was designed through *in situ* pyrolysis of g-C_3N_4, as shown in Figure 3c.[110] In this synthesis process, porous carbon was obtained from pyrolysis of potassium citrate at 800 °C. Then, iron (III) nitrate nonahydrate, porous carbon, and α-D-glucose were mixed to get a slurry. After drying at 60 °C, the slurry was ground together with melamine at a mass ratio of 1:5. Finally, the mixture was annealed at 800 °C in an Ar atmosphere for 2 h to obtain Fe SACs. During the synthesis process, the strong binding with N atoms, at a higher pyrolysis temperature, was critical for the stability of SACs with high loading. The single atom structure was confirmed by X-ray photoelectron spectroscopy (XPS) and XAS, which showed a similar structure with iron

phthalocyanine containing Fe–N_4 moieties. Interestingly, the obtained Fe-NC SACs showed a superior oxygen reduction reaction (ORR) performance, while Ni-NC SACs exhibited a high CO_2 reduction reaction activity.

From these studies, it was found that the specific structure (i.e., high-density N atoms, as well as six-fold cavities) of g-C_3N_4 can provide sufficient anchoring sites and, thus, trap the metal atoms during the synthesis process.[91] *In situ* generated metal-g-C_3N_4 intermediate will be decomposed to atomically dispersed M-N_x at a high temperature in an inert gas atmosphere. The metal loading in the obtained SACs is relatively high, due to the high N density. Numerous nitrogen-rich precursors can be used to generate g-C_3N_4, making this strategy promising for large scale synthesis of SACs with high metal loading.

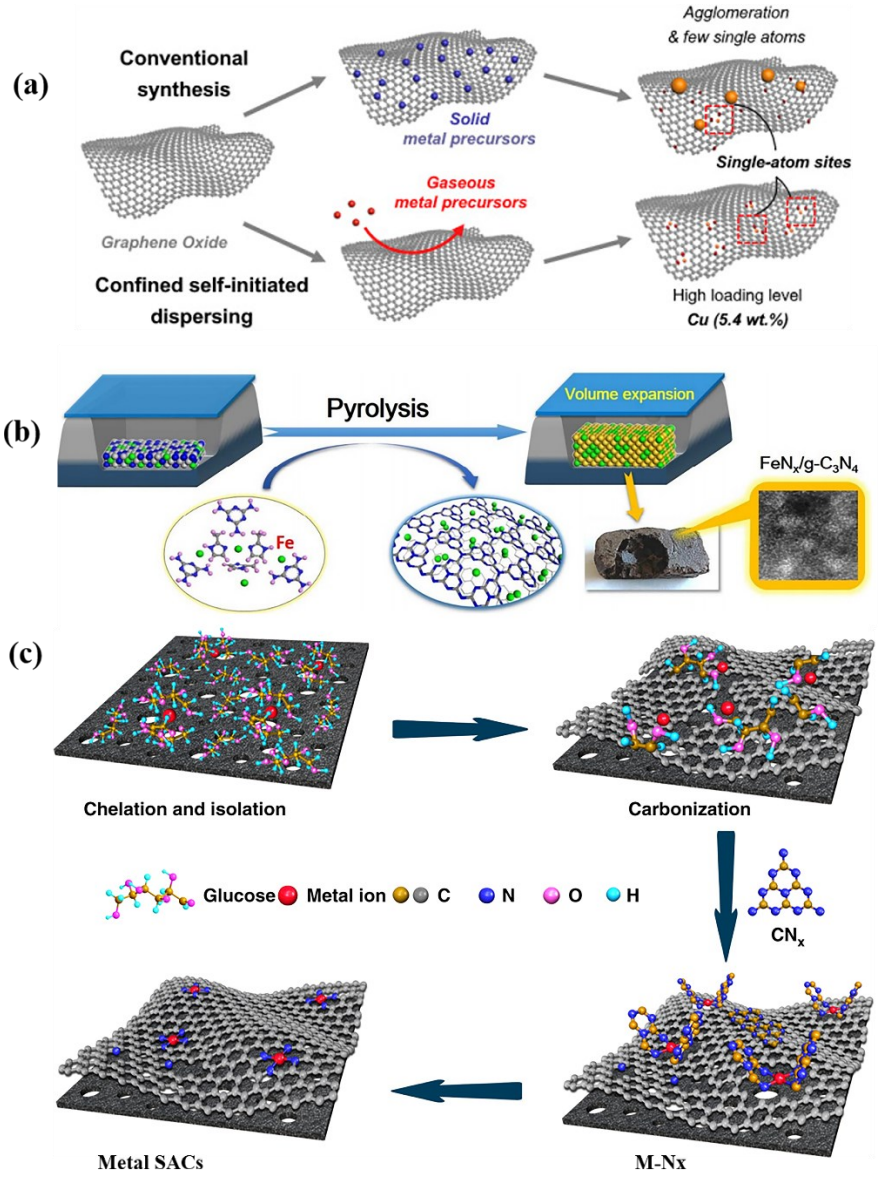

Figure 3. (a) Schematic illustration of Cu SACs on graphene,[109] reprinted with permission from ref [109], Copyright 2019 Elsevier Inc. (b) Preparation of $FeN_x/g\text{-}C_3N_4$ catalysts,[91] reprinted with permission from ref [91], Copyright 2018 American Chemical Society. (c) A general approach for the synthesis of different metal SACs,[110] reprinted with permission from ref [110], Copyright 2019 Nature Publishing Group.

2.1.3. Pyrolysis of *in situ* generated porous polymeric materials

Porous polymeric materials are suitable for the spatial confinement strategy, which can be *in situ* created to confine the metal precursors. For instance, Zhang et al. fabricated Ni SACs of 6.63 wt.%.

Ni content by decomposing the mixture of small organic molecules with Zn/Ni salts.[124] As shown in Figure 4a, Zn^{2+} first reacted with 2-methylimidazole (2-MeIm) to generate ZIF-8 and, then, Ni^{2+} absorbed within the pores of ZIF-8. At a higher temperature, DCD was converted to g-C_3N_4, capturing the released Ni^{2+} from the decomposition of ZIF-8. Both DCD and 2-MeIm played important roles during the synthesis. The obtained Ni SACs showed a high Faradaic efficiency (FE) of 97% and excellent stability for CO_2 electroreduction to CO. Bao et al. also got Ni SACs with 5.44 wt.% Ni loading by pyrolysis of ZIF-8.[125] The obtained catalysts with unsaturated Ni–N sites simultaneously achieved high current density and FE of the CO_2 reduction reaction. Similarly, Co SACs with a high loading of 15.3 wt.% were obtained by pyrolysis of KCl particles wrapped with a Co-based organic framework (ZIF-67), as shown in Figure 4b.[126] Co^{2+} and 2-MeIm were used to grow a thin layer of ZIF-67 on the surface of KCl particles. Then, the ZIF-67 wrapped KCl particles were annealed in an Ar atmosphere at 750 °C for 2 h. Finally, the obtained products were washed with a HCl solution and diluted water. The resulting Co SACs showed superior bifunctional catalytic activities toward ORR.

Surfactants can also play an important role during SACs synthesis. Zhou et al. prepared Pt SACs, with metal loading of 12.0 wt.%, with the assistance of a surfactant.[89] The success resulted from the unique structure of MOF, with an ultrathin 2D structure, with a thickness of 2.4±0.9 nm and a high surface area of 570 $m^2 \cdot g^{-1}$, that provided sufficient accessible active sites. The synthetic route is shown in Figure 4c. Polyvinyl pyrrolidone (PVP) molecules selectively attached to the surface of MOF pieces, and significantly allayed their stacking, forming 2D MOF nanosheets.[127-128] In contrast, only bulk MOF crystals were produced without surfactants.[129-132] The obtained Pt SACs exhibited distinguished photocatalytic activity for H_2 evolution through water splitting under visible-light, and the catalysts remained 93% of the initial activity after four cycles of reaction, indicating good stability.

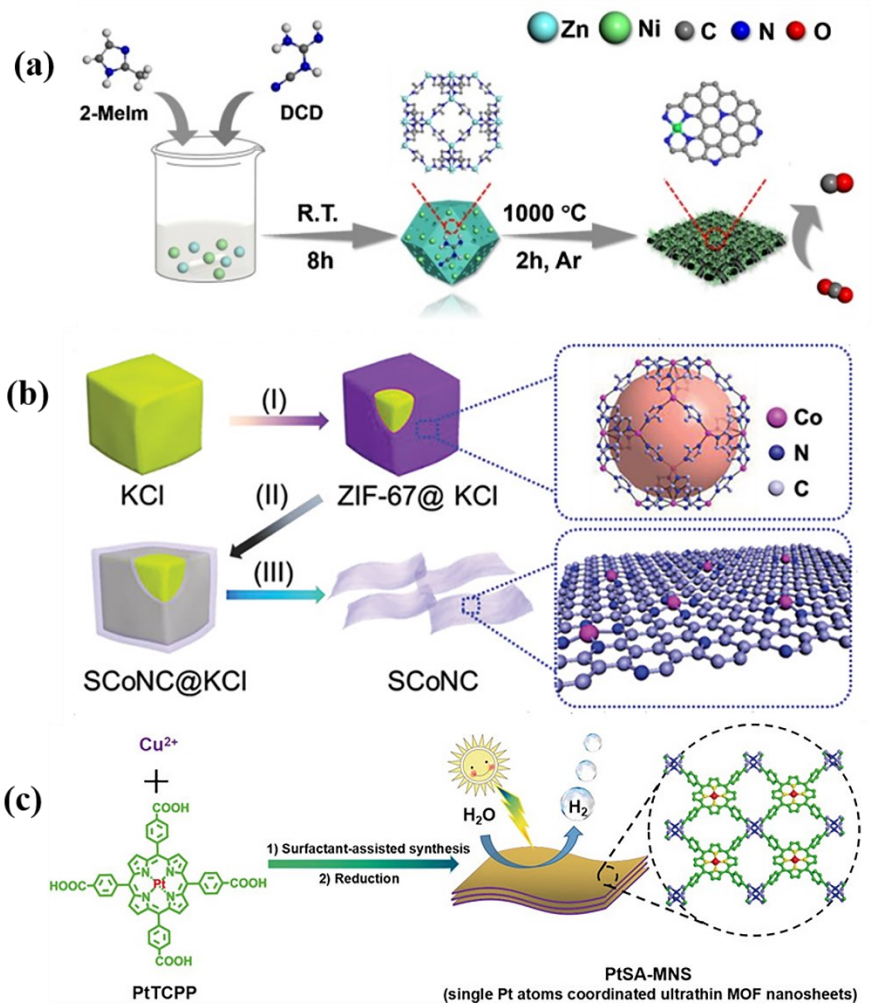

Figure 4. (a) Scheme for the synthesis of Ni SACs,[124] reprinted with permission from ref [124], Copyright 2019 Elsevier Inc. (b) Scheme for the synthesis of Co SACs,[126] reprinted with permission from ref [126], Copyright 2019 John Wiley and Sons. (c) Illustration of the synthetic path towards PtSA-MNS,[89] reprinted with permission from ref [89], Copyright 2019 John Wiley and Sons.

As an analogy to MOFs, CTFs can also be used to prepare SACs with high loading because of their abundant nitrogen sites. Cao et al. prepared Co SACs with 5.15 wt.% loading[112] and Fe SACs with 8.3 wt.% loading[113] by incorporating Co/Fe porphyrin-like units into CTFs and subsequent *in situ* pyrolysis. As shown in Figures 5a and 5b, CTFs were formed by trimerizing of the metal precursors at 400 °C. Then, the formed CTFs were converted *in situ* into Co/Fe porphyritic triazine-based carbonaceous (PTFs) at elevated temperatures. Finally, atomically dispersed M–N_4 structures were achieved.

These examples demonstrate that porous polymeric materials can not only provide coordination sites for anchoring metal atoms,[112-113, 133] but they can also encapsulate the metal precursor in the cage against migration and agglomeration.[102, 124] By thermal treatment of the cage encapsulated metal precursors, SACs with high metal loadings can be obtained.

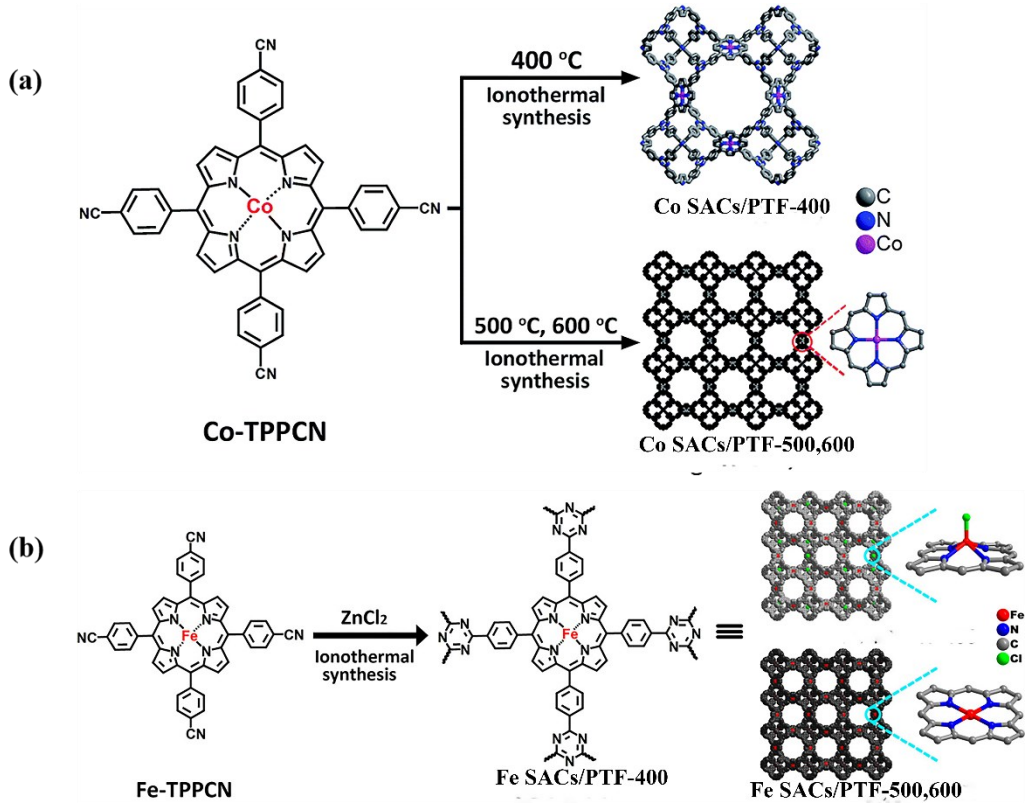

Figure 5. (a) Synthesis of Co SACs/PTFs,[112] reprinted with permission from ref [112], Copyright 2019 Royal Society of Chemistry. (b) Synthesis of Fe SACs/PTFs,[113] reprinted with permission from ref [113], Copyright 2018 American Chemical Society.

2.2. S-contained substrates

Besides N-contained substrates, S-contained substrates are also utilized to prepare high metal loading SACs. The metal-sulfur interaction is actually stronger than metal-nitrogen interaction,[134] showing promise for stabilizing the metal species firmly. However, substrates with high S density are not as easily obtained as substrates with high N density. Several attempts have been made to fabricate substrates with high S density. For instance, Choi et al. prepared a S-doped zeolite-templated carbon (ZTC) with 17 wt.% of S by chemical vapor deposition of acetylene/H_2S in NaX zeolite at 550 °C, followed by H_2S/He or pure He treatment at 800 °C. The unique carbon structure

could stabilize the atomically dispersed Pt as high as 5 wt.%.[99] The zeolite was further removed by HCl/HF dissolution. The unique carbon microstructure facilitated the formation of highly S-coordinated Pt structures, that is, Pt-S_4 [135] (as shown in Figure 6a), confirmed by XAS in combination with the density functional theory (DFT) calculations. Moreover, the synthesized carbon was physically flexible, allowing effective Pt coordination with the carbon framework.[136] Atomically dispersed Pt SACs had a unique electrochemical behavior. The obtained Pt SACs went a $2e^-$ ORR way producing H_2O_2, rather than the $4e^-$ pathway, producing H_2O. The mechanism was confirmed by DFT, as electrocatalysis on Pt SACs was not thermodynamically controlled, but rather kinetically limited. Another work was done by Liang et al.[137] Mesoporous S-doped carbons (meso_S-C) with a high surface area (>1,000 $m^2 \cdot g^{-1}$) , a high pore volume (> 2.0 $cm^3 \cdot g^{-1}$), and a high S loading (> 10 wt.%) were used to atomically disperse noble metals with metal loadings up to 10 wt.%, as shown in Figure 6b. Meso_S-C was prepared through cobalt-assisted carbonization of a molecular precursor. The unique structure of meso_S-C can effectively protect metal atoms from sintering during the pyrolysis process, owing to the robust metal-sulfur interactions. Although mesoporous O-doped, N-doped carbons, as well as carbon black, can also offer anchor sites for binding Pt atoms, the interactions between these heteroatoms and Pt was much weaker than those in the mesoporous S-doped carbons.[138-140]

Metal sulfide, with high resistance to carbon or sulfur poisoning, is another promising substrate for anchoring metal species. For example, Zeng et al. automatically deposited Pt on MoS_2 nanosheets with a metal loading of up to 7.5 wt.%.[23] In the synthesis process, Mo atoms in the MoS_2 nanosheets were replaced by Pt atoms. The structure was confirmed by HAADF-STEM and XAS. The white line intensity of Pt/MoS_2 decreased as the Pt loading increased from 0.2 wt.% to 7.5 wt.%, but it was still higher than that of Pt metal reference, indicating an oxidized Pt species. The oxidation state of the Pt species remained almost unchanged after CO_2 hydrogenation reaction, indicating high stability of Pt/MoS_2. Metal sulfide is also a good electronic conductor, which can be used in electrochemistry. For instance, Pt was atomically dispersed on amorphous CuS_x support (h-Pt_1-CuS_x) with a high concentration of single atomic Pt sites (24.8 at.%).[83] The obtained Pt SACs showed an ultrahigh productivity of H_2O_2 in electrochemical direct synthesis of H_2O_2 from H_2 and O_2. The affinity between Pt-S (shown in Figure 6c) was stronger than that of the Pt-O or Pt-N, preventing the formation of Pt clusters.[134]

The main disadvantage of using S-doped substrates is the utilization of H_2S and HF during the treatment, which are highly toxic. Multiple steps are needed to obtain the S-doped substrates, limiting the large-scale synthesis of high metal loading SACs. Because a high quality MoS_2 nanosheet requires strict operating conditions, it is not appropriate for low-cost and large-scale production.

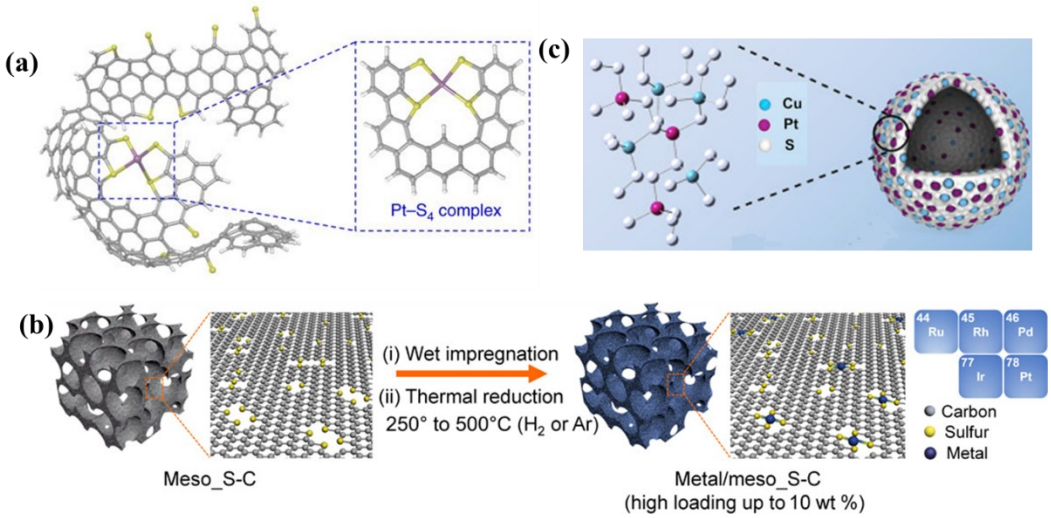

Figure 6. (a) Proposed structure of Pt-S_4,[99] reprinted with permission from ref [99], Copyright 2016 Nature Publishing Group. (b) Different noble metals atomically deposited on meso_S-C,[137] reprinted with permission from ref [137], Copyright 2019 American Association for the Advancement of Science. (c) Structure of h-Pt_1-CuS_x,[83] reprinted with permission from ref [83], Copyright 2019 Elsevier Inc.

2.3. O-contained substrates

Besides N and S, oxygen can be used to anchor metal species as well. Metal oxides are preferred substrates for electrochemical applications owing to their conductivity. Lee et al. synthesized Pt SACs with 8 wt.% metal loading on antimony-doped tin oxide (ATO).[141] Pt SACs were synthesized by an incipient wetness impregnation method and reduced at 400 °C under 10 vol.% H_2. The dispersion of Pt atoms was highly dependent upon the reduction temperature. Pt NPs were formed when the reduction temperature was 100 °C, while Pt SACs were obtained when the reduction temperature was 400 °C. The obtained Pt SACs showed different catalytic behaviors from that of Pt NPs. In a formic acid oxidation reaction, Pt SACs followed a direct path, while Pt

NPs followed an indirect path. As for the ORR, Pt SACs went for the 2 e^- path, whereas Pt NPs went for the 4 e^- path.

Layered double hydroxides (LDHs) also contain O atoms and can be used to fix metal species. Song et al. designed a Ru SAC with 7 wt.% metal loading on a monolayer NiFe-LDH.[142] Monolayer NiFe–LDH was prepared *via* a one-step co-precipitation method. Single Ru atoms, dispersed on monolayer NiFe–LDH, were synthesized *via* a similar one-step co-precipitation method in a formamide solution. The Ru single atoms exactly occupied on the top of the Fe atoms through three O atoms, rather than dispersed randomly in the LDH structure. The precise location of single Ru atoms lowered the reaction barrier energy, and thus enhancing hydrazine electrooxidation.

Carbon materials usually contain oxygen-containing groups on the surface. Uzun et al. prepared iridium (Ir) SACs with 14.8 wt.% metal loading by the reaction of $Ir(CO)_2(acac)$ with oxygen-containing groups on a reduced graphene aerogel (rGA) in anhydrous toluene.[143] The whole preparation was conducted in air-exclusive conditions. The high metal loading resulted from rGA's high surface area and a high density of sites for anchoring Ir species. Moreover, rGA had a better electron donor character than most of metal oxides.

So far, there are only a few reports concerning the preparation of SACs with high metal loading on metal oxides, due to relatively weak metal-oxygen interaction. It would be excellent if metal oxides with wide industrial applications could be used as the substrates. Smarter strategies should be developed to make metal oxides suitable for the synthesis of high metal loading SACs.

3. Characterization of SACs

Advanced characterization techniques are critical for successfully researching SACs, because supported SACs can barely be observed by conventional characterization methods (e.g., regular TEM) due to their limited instrument resolution. Therefore, advanced characterization techniques are urgently needed for the study of SACs to provide direct evidence and confirmation of their structural and electronic properties. Fortunately, recent advances in electron microscopy allow researchers to directly observe the structural transformation of SACs, facilitating the investigation of their physical-chemical essence and the mechanisms of the synthesis process. For example, AC-HAADF-STEM, with atomic resolution, can be used to directly observe the distribution of SACs.[44] XAS measurement is used to get detailed information on the local electronic and atomic

structure of SACs. Moreover, DFT calculations, combined with the above-mentioned characterization methods, can provide reliable models of active centers.[28]

3.1. Electron microscopy with atomic resolution

Prior to the era of AC-HAADF-STEM, it was a major challenge to observe SACs on supports. Gates et al. first reported pioneering work on the identification of individual Ir atoms on MgO with AC-HAADF-STEM, which opened the door to direct visualization of single atoms.[144] AC-HAADF-STEM, with atomic resolution, is highly sensitive to variations in the atomic number (symbol *Z*), and can observe the dispersion and configuration of metal atoms on substrates. Metal atoms, with a higher *Z*, appear brighter in HAADF images.

Due to its ability to characterize SACs, Zhang et al. adopted the AC-HAADF-STEM with atomic resolution to directly observe Pt SACs with 0.17 wt.% of Pt.[20] As clearly shown in Figure 7a, Pt atoms were atomically distributed on the surface of FeO_x. Only Pt single atoms were observed after examining different regions of the sample. Figure 7b shows that individual Pt atoms occupied exactly the positions of the Fe atoms. By adjusting beam focus settings, the authors confirmed that single Pt atoms were on the surface of FeO_x. Moreover, by statistically examining many HAADF images, the density of Pt single atoms was calculated to be about 0.07 Pt atoms per nm^2, closing to actual Pt loading. Liu also explored the AC-HAADF-STEM to observe Pt_1/Fe_2O_3.[44] As can be seen in Figure 7c, all Pt single atoms were dispersed atomically. However, the various configurational heterogeneity of Pt single atoms can be observed. Yellow arrows indicate isolated Pt atoms, yellow block arrows indicate loosely connected and atomically dispersed Pt “clusters”, and the white arrow indicates other types of Pt configurations. This phenomenon was rarely observed when the metal loading was low. The reason could be due to different types of anchoring sites for fixing the metal atoms during the synthesis process.[145] The dispersion of single atoms in high metal loading samples can also be observed through AC-HAADF-STEM. Zn SACs with 9.33 wt.% of Zn[114] and Co SACs with 15.3 wt.% of Co[126] can be clearly seen in Figures 7d and 7e, respectively. According to the inset in Figure 7e, 96.1% of Co dots were in the range of 0.1-0.2 nm, showing the high dispersion even at high metal loadings.

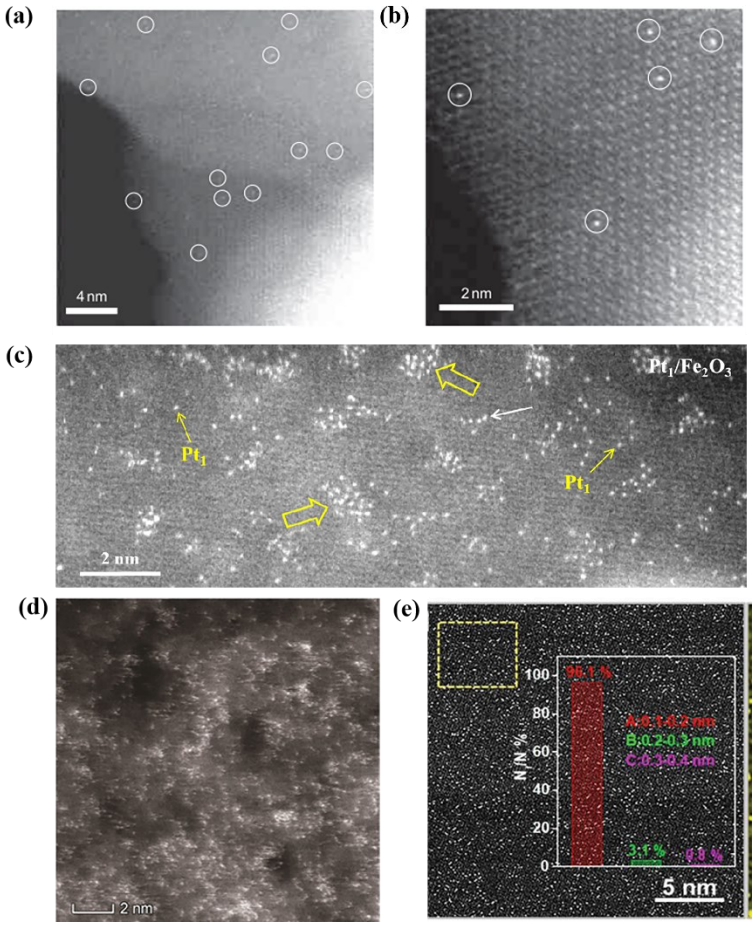

Figure 7. AC-HAADF-STEM images of Pt_1/FeO_x: (a) Pt single atoms were individually distributed on FeO_x, (b) Pt single atoms substituted the Fe atoms exactly,[20] reprinted with permission from ref [20], Copyright 2011 Nature Publishing Group. (c) various configures of Pt single atoms,[44] reprinted with permission from ref [44], Copyright 2017 Elsevier Inc. (d) AC-HAADF-STEM image of Zn SACs with 9.33 wt.% of Zn,[114] reprinted with permission from ref [114], Copyright 2019 John Wiley and Sons. (e) AC-HAADF-STEM image of Co SACs with 15.3 wt.% of Co, where the white dots are Co atoms. The inset is the range of Co atoms diameter, indicating most of the Co atoms are independent.[126] Reprinted with permission from ref [126], Copyright 2019 John Wiley and Sons.

Although AC-HAADF-STEM was powerful for examining the dispersion of SACs, it is still difficult to monitor reactions catalyzed by SACs in severe gas environments and operating temperatures using *in situ* imaging techniques. It would be helpful if the dynamic behavior of single atoms could be tracked directly during the reactions, which would be useful in identifying

the active center as well as the deactivation mechanisms caused by migrating. Thus, Li et al. combined AC-HAADF-STEM with *in situ* TEM to observe the formation of Ni SACs from Ni NPs.[146] As shown in Figures 8a-8c, the transformation from Ni NPs to Ni SACs can be gradually completed in the first 3 h, accompanied with the explosion of surface holes. The obtained pores and Ni SACs can be retained even after annealing for another 3 h (Figure 8d), demonstrating high stability. Figure 8e represents *in situ* TEM images acquired at 900 °C, showing that, at the initial stage, a Ni NP was confined in a hole of N-rich amorphous carbon layer, with a diameter of 4.8 nm. The NP, downsized to 4.6 nm at 30 s, rapidly reduced to 1.6 nm in the following 6 s, and disappeared in the next 14 s, together with the generation of surface holes. Similar work was also done by Zhang et al., that recorded the disintegration of Pt NPs to Pt SACs by high-temperature calcination, using *in situ* HAADF-STEM.[147] The observed disintegration process was different from the reported Ostwald Ripening mechanism,[148] indicating the power of *in situ* HAADF-STEM in understanding synthesis mechanisms.

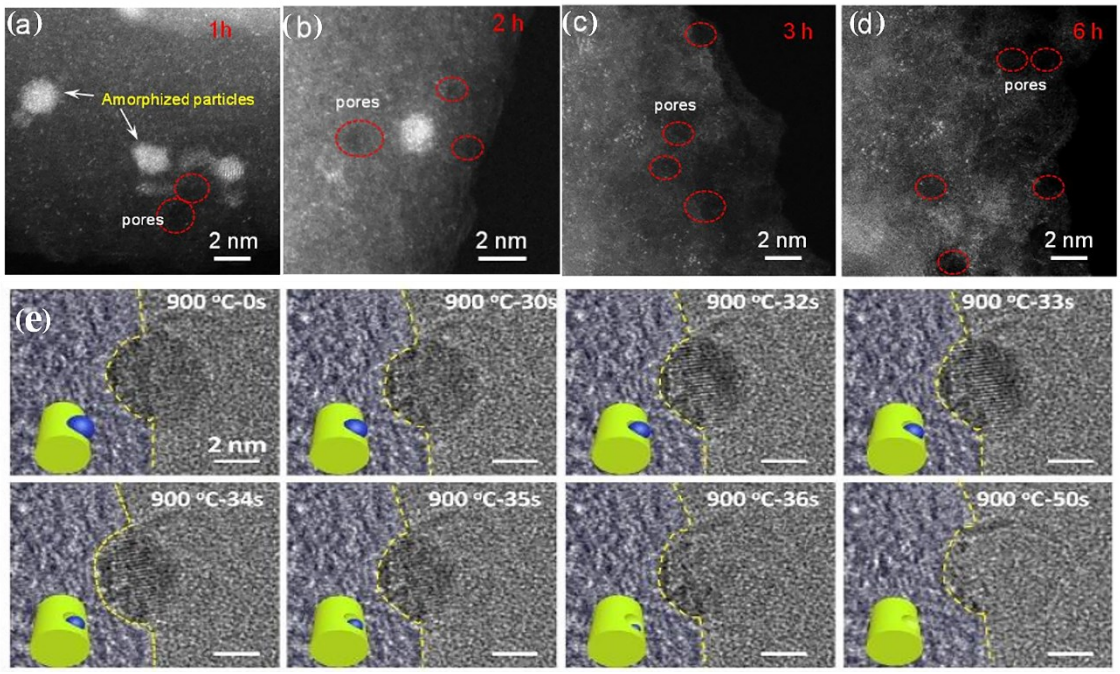

Figure 8. (a)-(d) AC-HAADF-STEM images of Ni SACs, and (e) *in situ* TEM images of the evolution from Ni NPs to Ni SACs.[146] Reprinted with permission from ref [146], Copyright 2019 John Wiley and Sons.

Although some achievements have been obtained, challenges remain in the field of *in situ* TEM. The main issue for *in situ* imaging techniques comes from the scattering phenomena relative to the gas cell geometry and electron-beam induced effects.[44] Gai and Boyes first used an atomic resolution environmental transmission electron microscope (atomic resolution ETEM) to show the sintering of Pt particles on TiO_2.[149] This clearly demonstrated the shift from finely dispersed Pt particles at room temperature to Pt clusters under a reaction environment. *In situ* results indicated an increase of Pt particle size and metal support interactions with the increase of reduction temperature that was conducive to understanding Pt dispersion, the role of Pt size in strong metal–support interactions, and the fraction of Pt available for gas reaction. To study the influence of the reaction gases, the same group conducted *in situ* studies of dynamic Au and Pt nano catalyst reactions under designed gas atmospheres and temperature at the atomic level.[150] Results indicated that the mobility of Pt single atoms was both gas and temperature dependent. An *in situ* observation of the evolution of Au clusters from Au single atoms in a WGS reaction was also done by the same group, indicating the necessity for anchoring sites of support materials to stabilize single atom species.[67]

Li et al. recorded the conversion of noble metal NPs into highly thermal stable SACs, above 900 °C in an Ar atmosphere, using *in situ* ETEM.[151] During the conversion, the atomization and agglomeration processes were confirmed to coexist, and the atomization eventually won the competition with the assistance of -CN functional groups. Notably, the identified atomic structure (PdN_4) of Pd SACs shared certain similarities with the reported non-noble MN_4 structure, which inferred that the same strategy could be applied to conventional metal-N_4 materials.

So far, it is still challenging to fully understand the three-dimensional (3D) distribution of individual atoms, especially for SACs supported on mesoporous materials. Usually, an electron microscope provides a 2D projection image of a 3D object, causing a loss of 3D information during the imaging process. Thus, it is essential to obtain 3D images of supported SACs and to reliably analyze the true spatial distribution of the SACs. Some efforts[152-153] have been made to collect 3D information on supported metal catalysts and particle size distributions. Jong et al. utilized the HAADF mode to obtain 3D information of palladium-ruthenium on mesoporous silica.[152] Unfortunately, the resolution was still in the nanometer scale, at that time, which was not high enough for single atoms supported on mesoporous materials. Thus, Ortalan et al. used the AC-HAADF-STEM with atomic resolution to image Ir single atoms supported on de-aluminated

zeolites.[154] Due to the limitation posed by the beam-sensitive property of zeolites, low-dosing conditions (minimal exposure to an electron beam) were required. Although Ir single atoms inside the pores of the zeolite were observed by the AC-HAADF-STEM, the signal-to-noise ratio was poor due to the low-dose conditions. Therefore, Han et al. developed an integrated differential phase-contrast scanning transmission electron microscopy (iDPC-STEM) to directly probe guest molecules on isolated single Mo clusters, supported on various zeolites with a high signal-to-noise ratio.[155] According to the positions of Mo atoms, the specific one-to-one Mo-Al interaction made it possible to locate Al atoms. The utilization of the iDPC-STEM provided a way to investigate, in unprecedented detail, the host-guest interactions in porous materials. However, the iDPC-STEM can only identify guest molecules under low-dose conditions.

To address the challenge of beam-sensitive zeolites, recent work done by Ulm University's Sub-Angstrom Low-Voltage Electron Microscopy (SALVE) project using 80 keV AC-HRTEM would be helpful. The group utilized low-voltage electron microscopy to show that the Pt nanocluster acted as a viscous liquid dispersing to single atoms and then re-clustering overtime during the reaction.[156] Direct observation of the dynamic nature of NPs and individual atoms can be harnessed to tune the performance of SACs. The development of low-voltage electron microscopy accelerated the *in situ* imaging technique, especially for beam-sensitive samples. The emergence of cryogenic electron microscopy can be a good choice, which enables the nondestructive characterization of electron-beam sensitive materials at atomic resolutions.[157] With the development of sample holders, electro detectors, and image reconstruction algorithms, the capability of characterizing SACs using electron microscopy will be significantly enhanced, and possibly lead to new more accurately SACs designs.

3.2. Scanning tunneling microscopy (STM)

STM is another powerful surface imaging instrument, with lateral and depth resolution of 0.1 nm and 0.01 nm, respectively.[53] The advantage of STM is that it can work under various conditions, such as air, water, and other liquids or gas ambient at a wide range of temperatures. Thus, STM has the ability to image single atoms under various working conditions, opening up a new way for structural and reactivity studies of SACs. For example, Parkinson et al. confirmed the dual role of CO in stabilizing sub-nano Pt clusters on the $Fe_3O_4(001)$ surface using time-lapse STM.[57] As shown in Figures 9a and 9b, two configurations, labeled as Pt_1 and Pt_1^*, were confirmed. Pt_1^*

gradually transferred to Pt_1 configuration, due to the higher binding energy of Pt_1 calculated from DFT. When the samples were exposed to 2 x 10^{-10} mbar CO, Pt clusters were observed (as shown in Figures 9c and 9d), with the majority of clusters containing two or three Pt atoms. Hence, CO not only led to the agglomerations of single Pt atoms into sub-nano clusters, but also stabilized the smallest clusters against decay, providing a strategy for designing stable SACs.

Moreover, STM enables the capture of the active center during a low-temperature CO oxidation, catalyzed by Pt SACs on Cu_2O.[56] By annealing at different temperatures, the authors confirmed that lattice oxygen, in close vicinity to the Pt species, was involved in the reaction process. Furthermore, STM has the ability to create desired nanostructures through manipulating single atoms in a precise way. Several works have been produced by Stroscio et al. from the Center for Nanoscale Science and Technology.[158-160] The ability to control the transfer of a single atom between lattice sites can lead to a better understanding of the electronic and geometric structure of SACs. Therefore, the development of STM will significantly benefit the SACs research. So far, it is still impossible to place single atoms at any desired locations to create desired structures.

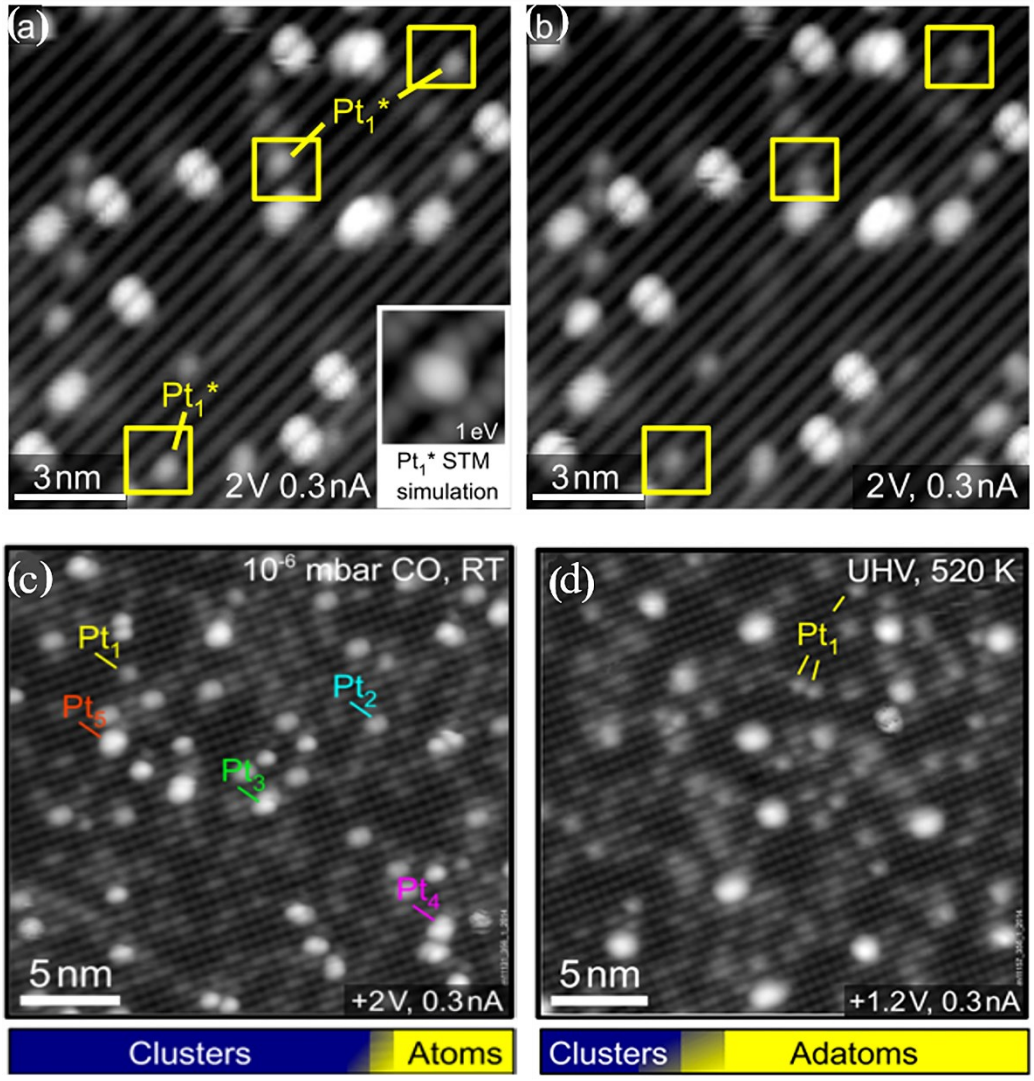

Figure 9. Time-lapse STM of the transfer of Pt configurations.[57] Reprinted with permission from ref [57], Copyright 2016 National Academy of Sciences.

3.3. X-ray absorption fine structure (XAS)

Typically, XAS is divided into two energy regions: X-ray absorption near-edge structure (XANES), and extended X-ray absorption fine structure (EXAFS). XANES can be used to identify oxidation state and coordination symmetry of metal, while EXAFS can be used to obtain accurate metal-ligand distances, as well as a coordination number via Fourier transform (FT) analysis. For example, XAS was employed to detect the oxidation state and coordination pattern of Fe SACs.[104, 110] According to Figures 10a and 10b, the Fe K-edge of FeN_4/GN samples resembled the original FePc reference curve, indicating that FeN_4/GN had the same valence state and the coordination

environment as that in the reference FePc. The structure was estimated as FeN_4 structure in FePc. Similarly, Hutchings et al. confirmed that the obtained Au/C materials contained no metallic Au–Au bond, and were consistent with the isolated Au chloride species, as shown in Figure 10c.[161] Linear combination fitting (LCF) of XANES (in Figure 10d) showes that Au species were presented in a mixed cationic form: 23% Au(III) and 77% Au(I).

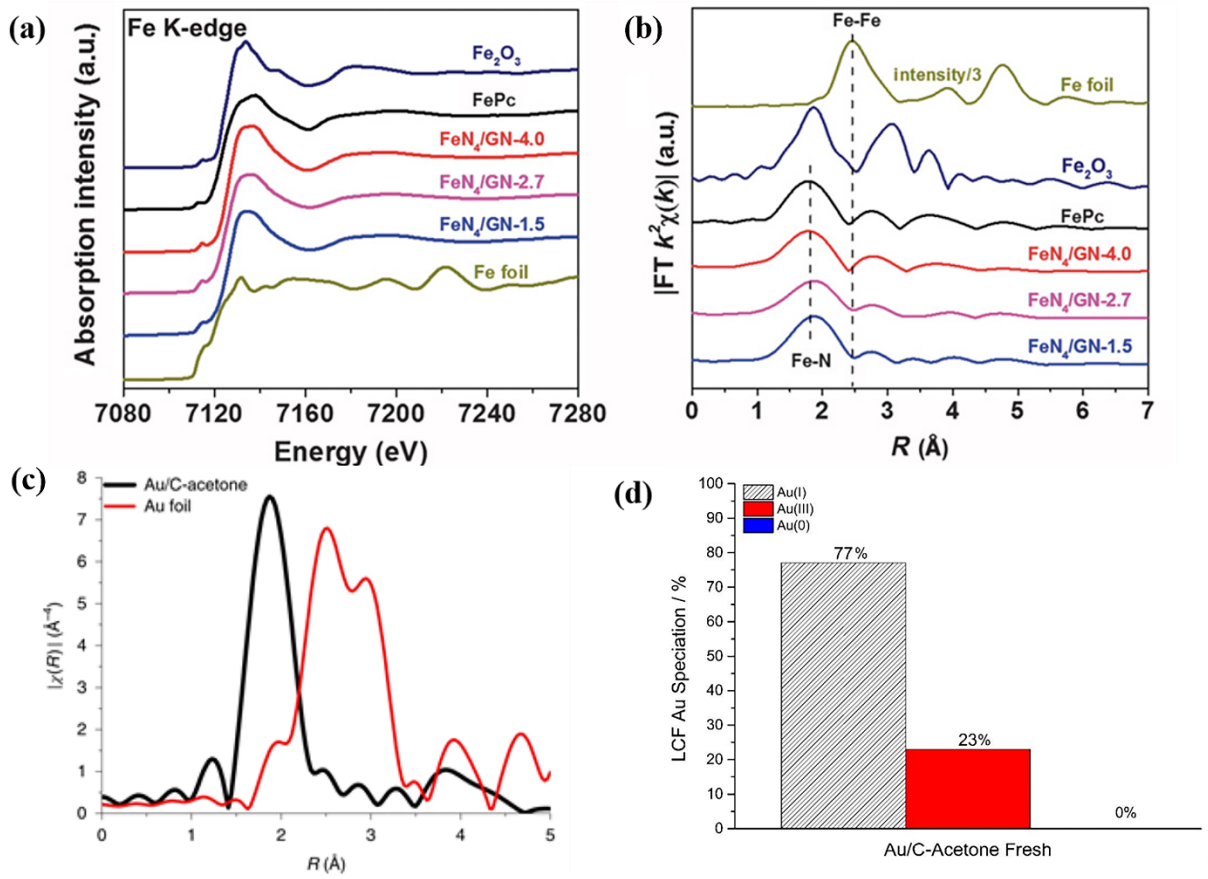

Figure 10. (a) XANES of Fe K-edge, (b) Fourier transform (FT) EXAFS of FeN_4/GN,[104] reprinted with permission from ref [104], Copyright 2015 American Association for the Advancement of Science. (c) FT-EXAFS spectrum of the 1 wt.% Au/C material, (d) LCF of the Au L_3-edge XANES.[161] Reprinted with permission from ref [161], Copyright 2020 Nature Publishing Group.

In situ and operando XAS provide access to investigating the dynamic process of the evolution of geometric and electronic structures at an atomic scale.[162-163] For example, Sun et al. performed *in situ* and operando XAS to monitor the structural and chemical state changes of Ru,

Co, and Fe species in the Ru/CoFe-LDHs catalyst under electrochemical conditions.[164] As can be seen in Figure 11, Ru species showed a reversible change of valence state. Ru K-edge went to a higher energy state, when the applied potential increased, but it went back to the initial value when the applied potential went back to open-circuit voltage (OCV). In contrast, both Co and Fe showed a higher chemical state when the applied potential went back to OCV, indicating the irreversible change of Co and Fe. The bonding lengths of Co/Fe–O shrank during the oxygen evolution reaction. Those changes were irreversible, further fixing a Ru atomic structure on the surface. Therefore, *in situ* and operando XAS is a useful technique for observing reaction induced structure change, and for facilitating an understanding of the activity, stability, and selectivity of SACs.

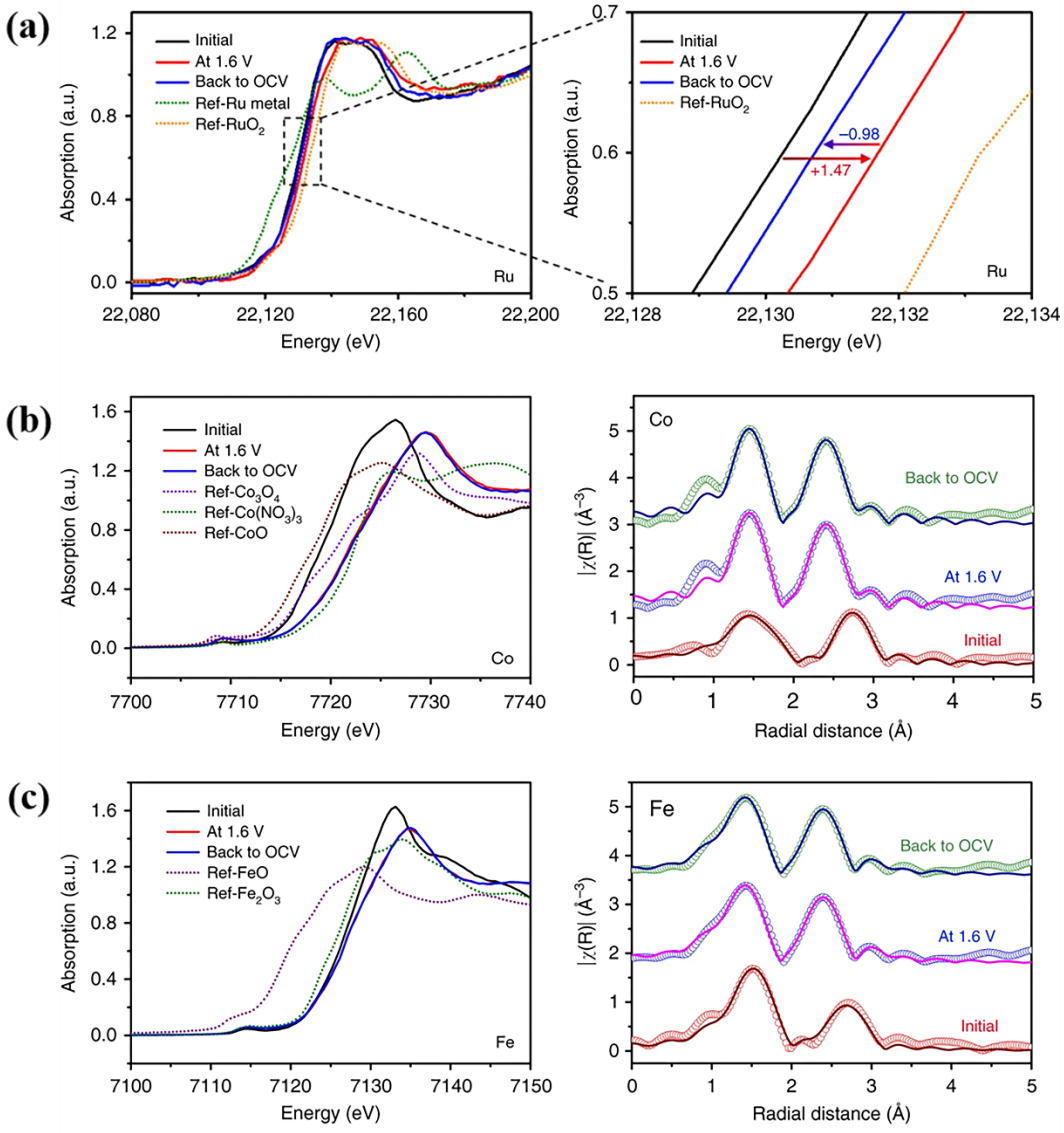

Figure 11. Operando XAS measurement of Ru/CoFe-LDHs in an electrochemical condition.[164] Reprinted with permission from ref [164], Copyright 2019 Nature Publishing Group.

Moreover, it is highly desirable to monitor the structure changes in a reactant gases condition. *In situ* and operando XAS has been used in hydrocarbon processing[40, 165-166], CO oxidation,[132, 167-171] and WGS reaction[172] to capture the dynamic process. For example, Gates et al. investigated the structure changes of zeolite-supported rhodium (Rh) SACs under different ethene/hydrogen (C_2H_4/H_2) ratios, using *in situ* and operando XAS.[165] The experiment was carried out in an EXAFS cell at 30 °C and 1 bar. When an ethene-rich mixture (4:1:5 C_2H_4/H_2/He) flew through the catalysts, *n*-butenes were the major products. The Rh SACs were stable under this condition, since no Rh-Rh contributions (no clusters) were detected by EXAFS spectroscopy. However, when the gases switched to pure H_2, a Rh-Rh contribution gradually grew and reached a final coordination number of 1.9, indicating the formation of Rh clusters. This work demonstrated that the regulation of the structure (switching between Rh SACs and Rh clusters) allowed fine-tuning of selectivity simply by variation of the feed composition.

More examples of the XAS technique being used to identify the nature of SACs can be found,[1, 72, 78] since it is powerful and essential for identification of local geometric and electronic structure of SACs. However, the wide application of this technique is not possible, due to the requirement of synchrotron radiation sources. The interpretation of the obtained absorption spectra is also complicated. Without rigorous theoretical methods, inaccurate spectral simulations may be obtained.

3.4. Fourier transform infrared (FTIR) spectroscopy

With appropriate probe molecules, FTIR spectroscopy is employed to confirm the presence of SACs and even quantify the dispersed SACs. The advantages of FTIR spectroscopy include quantification and *in situ* monitoring.[173] Combined with AC-HAADF-STEM, XAS, and DFT, FTIR offers a powerful toolbox for SACs study.

For the characterization of SACs, CO is an ideal probe. The behavior of CO adsorption on a metal surface has been widely studied.[174] CO can form a linear adsorption geometry as well as a bridging adsorption geometry.[175] The bridging adsorption geometry requires two metal atoms, indicating the existence of metal NPs. Therefore, the absence of bridging adsorption geometry can

be used to confirm the presence of single atoms. For example, Ding et al. used CO probe molecule FTIR to differentiate the existence of Pt single atoms from Pt NPs.[58] The IR peaks at 2,115 cm^{-1} and 2,070 to 2,090 cm^{-1} (in Figure 12a) were assigned to CO adsorbed on Pt single atoms and Pt NPs, respectively. Pt single atoms behaved as spectators, while Pt NPs showed activity for CO oxidation and WGS reaction at a low temperature, as shown in Figures 12b and 12c. The inert activity of Pt single atoms resulted from strong CO adsorption. The addition of Na^+ greatly lowered the CO adsorption on Pt NPs, with more sites remaining to activate O_2 and H_2O. Hence, the performance of the catalyst with a WGS reaction was enhanced by the addition of Na^+.[176-179] Similarly, Zeng et al. used *in situ* pressure-dependent DRIFT to study the chemical states and coordination environments of Pt species in Pt/MoS_2.[23] The peak positions for CO on Pt SACs remained unaffected by a decrease in CO pressure, while those for CO on Pt NPs were red shifted by a decrease in CO pressure.

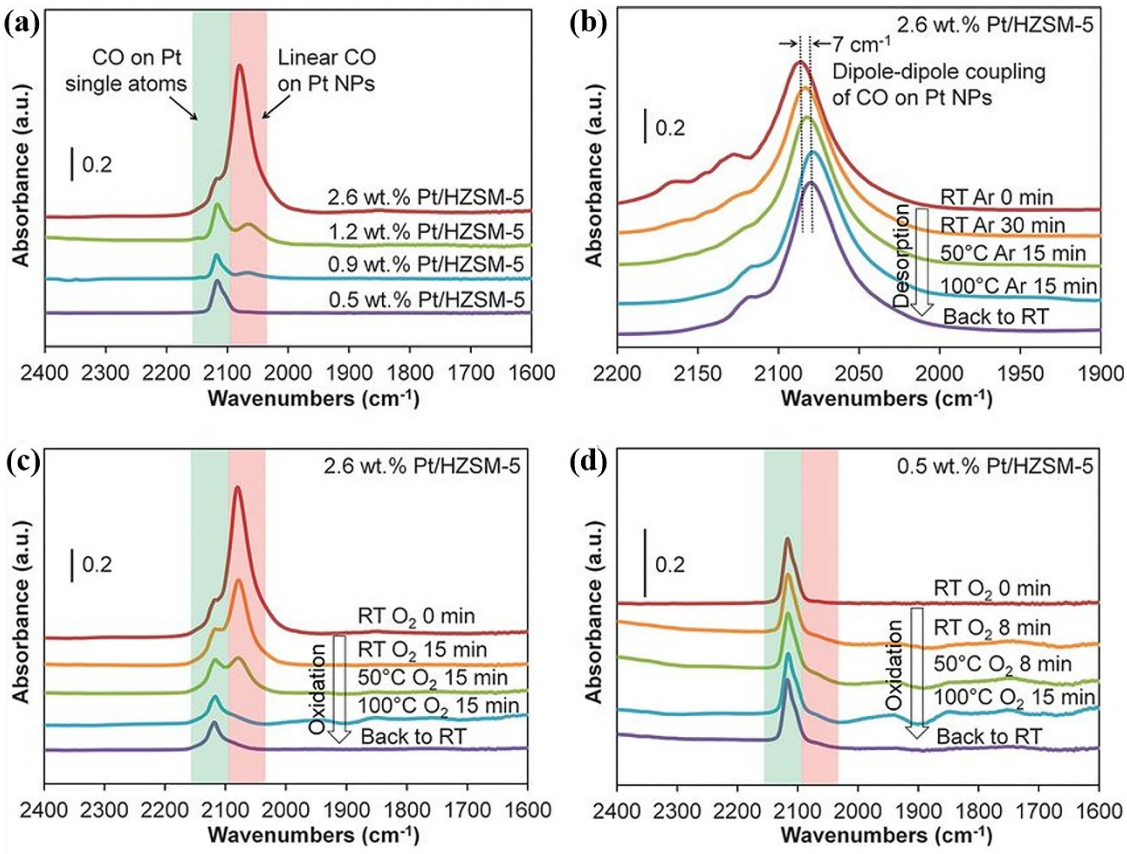

Figure 12. (a) FTIR spectra of CO adsorbed on Pt/HZSM-5 catalysts with different Pt loadings, (b) time-dependent FTIR spectra of CO adsorbed on Pt/HZSM-5 with 2.6 wt.% Pt, and time-

dependent FTIR spectra of CO adsorbed on (c) Pt/SiO_2 and (d) $Pt\text{-}Na/SiO_2$ upon H_2O exposure.[58] Reprinted with permission from ref [58], Copyright 2015 American Association for the Advancement of Science.

In situ DRIFT can also be used to investigate CO adsorption ability on Cu SACs.[180] Atomically dispersed copper species were constructed through calcination in air at 800 °C. The high temperature treated catalysts showed a stronger ability to adsorb CO than low temperature treated catalysts did. As shown in Figure 13a, the CO-Cu(I) peak at ~2,110 cm^{-1} of 1CuCe-400 (1 was the copper loading in weight percent and 400 was the calcination temperature with unit °C) was about 20 times weaker than that of 1CuCe-800. Peaks of CO_2 at ~2,362 and ~2,334 cm^{-1} immediately appeared as O_2 was introduced to 1CuCe-800 catalyst (1 was the copper loading in weight percent and 800 was the calcination temperature with unit °C), indicating rapid oxidation of CO-Cu(I) to form CO_2. The obtained catalyst exhibited a significant superiority in catalyzing CO oxidation, in that its CO consumption rate reached 6,100 $\mu mol_{CO} \cdot g_{Cu}^{-1} \cdot s^{-1}$ at 120 °C. This value was 30 times that of Pt/CeO_2.

The limitation of CO chemisorption DRIFTS is that it can only be applied to noble metal-based SACs. Non-noble metals usually have a weak interaction with CO. Besides, it is not suitable for carbon-based catalysts because of the strong light adsorption.[181]

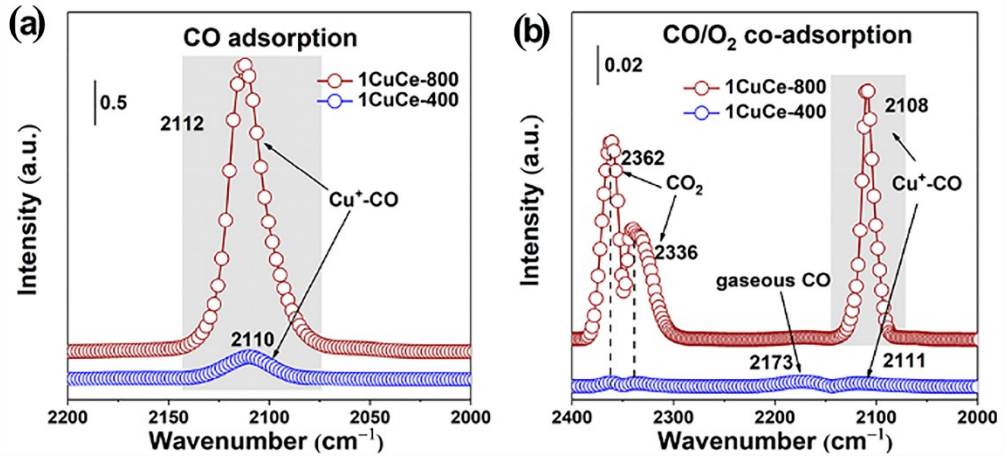

Figure 13. *In situ* DRIFTS spectra of 1CuCe-800 and 1CuCe-400 in (a) CO adsorption condition and (b) CO/O_2 co-adsorption conditions at 120 °C.[180] Reprinted with permission from ref [180], Copyright 2019 American Chemical Society.

3.5. Other technologies

Moreover, the rapid development of *in situ* ambient pressure XPS[182-183] and mass spectrometry[184-185] have also facilitated the research of SACs in realistic conditions. The theoretical calculation is another powerful tool for uncovering the fundamental catalytic reaction mechanisms of SACs.[186-187] A deeper understanding of the structures and active centers of the SACs can be achieved by a combination of theoretical calculations with advanced characterization techniques.

4. Understanding of Active Center

It is still a significant challenge to identify the active centers of NP catalysts, since the distribution of NPs is usually non-uniform. Therefore, the catalytic performance is the average outcome of all non-uniform active centers.[29] Fortunately, SACs provide an ideal model for investigating the active centers because of their definite structure characteristics. Although SACs maximize the dispersion of metal, a general question is whether atomically dispersed metal atoms can function as an active center to achieve the highest intrinsic catalytic performance. This fundamental question remains unanswered. Indeed, SACs are not always shown to be better than their NP counterparts by a closer examination of the activity per atom. Sometimes, SACs might completely inert or serve only as a spectator in reactions, especially for those that require two or more neighboring metal atoms to activate the reactants, in which case NPs will always be better than SACs.[28] Therefore, a in-depth investigation of the active center is imminent, since an optimal active center is critical for catalytic performance.

4.1. Single atom with neighboring atoms

Currently, the metal loading in SACs is generally kept below 1.0 wt.% to prevent sintering. Thus, single atoms are far apart due to the low loading, and the interaction between single atoms is generally ignored.[23] Therefore, one way to shorten the distance between single atoms is to increase metal loading, while maintaining the atoms as individual sites.

Zeng et al. obtained neighboring Pt single atoms by increasing the metal loading to 7.5 wt.%.[23] At lower Pt loadings, the distances between the nearest Pt single atoms were more than 3 nm. Electron transfer only occurred between a Pt atom and its bonded S atoms. Thus, every Pt

atom and the corresponding boned S atoms functioned as an “active center”. When the Pt loading increased, the “active centers” partly overlapped or were adjacent, forming neighboring Pt single atoms. In a CO_2 hydrogenation reaction, methanol was generated without the formation of formic acid over isolated Pt single atoms. However, CO_2 underwent a sequential transformation into formic acid and methanol over the neighboring Pt single atoms, showing different reaction paths. DFT was used to investigate the reaction paths, as shown in Figure 14. As for the neighboring Pt single atoms, the formation of HCOOH was more favorable than that of $C(OH)_2^*$, since the reaction barriers for the conversion of COOH* into HCOOH or $C(OH)_2^*$ were 1.01 eV or 1.34 eV, respectively. As for the isolated Pt single atoms, $COOH^*$ and CH_2OH^* were intermediates due to high transformation energy barriers. The intermediates were also confirmed by *in situ* DRIFT and XPS. As such, neighboring Pt single atoms worked together to alleviate the energy barriers, promoting catalytic performance. The synergetic interaction between neighboring single atoms was supposed to develop a new way to manipulate catalytic properties and advance the fundamental understanding of heterogeneous catalysis.

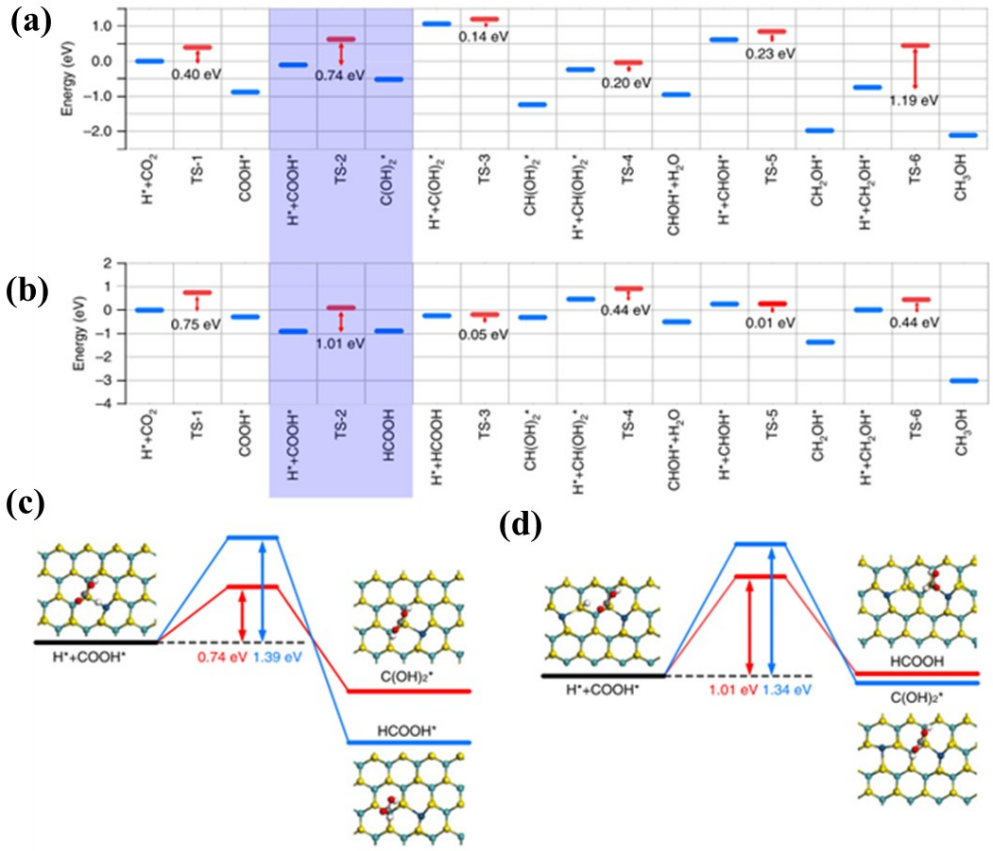

Figure 14. Optimized reaction paths in CO_2 hydrogenation for (a) Pt_1/MoS_2 and (b) Pt_{2iii}/MoS_2, and steps for the addition of a H atom to COOH* over (c) Pt_1/MoS_2 and (d) Pt_{2iii} $/MoS_2$.[23] Reprinted with permission from ref [23], Copyright 2018 Nature Publishing Group.

Yang et al. designed a Pt-O-Pt ensemble, using isolated Pt_1 single atoms on CeO_2 as "seeds".[188] To prepare a Pt-O-Pt ensemble catalyst, Pt_1/CeO_2 was first reduced in a mild H_2 atmosphere, followed by a CO plus O_2 treatment, thereby reconstructing Pt species. For the structure of Pt_1/CeO_2, the Pt single atoms preferred to replace the Ce atom on the ceria surface and a square-planar Pt_1-O_4 structure was identified. After the activation treatment, the structure were rearranged into a Pt_8O_{14} formation, containing Pt-O-Pt as the only catalytic base unit. EXAFS showed the typical exclusive Pt-O coordination pattern for Pt_1/CeO_2, and the Pt atoms of Pt-O-Pt/CeO_2 were only bridged by O atoms. As can be seen in Figure 15, the performance of a low-temperature CO oxidation, catalyzed by Pt-O-Pt ensemble, was 100-1,000 times more active than that of their isolated single atom Pt_1/CeO_2 parent. This resulted from a lower apparent activation

energy of the Pt-O-Pt/CeO_2 catalysts than that of the Pt_1/CeO_2 parent catalysts. Based on the DFT calculation, CO oxidation followed the Mars–van Krevelen mechanism for Pt_1/CeO_2 with a square-planar Pt_1-O_4 unit. The Pt-Ce interface was considered as the active center for CO oxidation over Pt_1/CeO_2. However, the Pt-Ce interface was not the active center for Pt-O-Pt/CeO_2. Interestingly, CeO_2 support in Pt-O-Pt/CeO_2 was a spectator. This work found that Pt-O-Pt facilitated the rapid migration of oxygen to catalyze CO oxidation. Pt-O-Pt assembles can be obtained through similar oxygen linkages while substrates, other than CeO_2, may also be used to create Pt-O-Pt. In order to valid this hypothesis, the authors successfully created a Pt-O-Pt unit on a La-Al_2O_3 support. In the future, further efforts should be made to fabricate exclusive active centers over various supports, providing a powerful platform for designing novel catalysts.

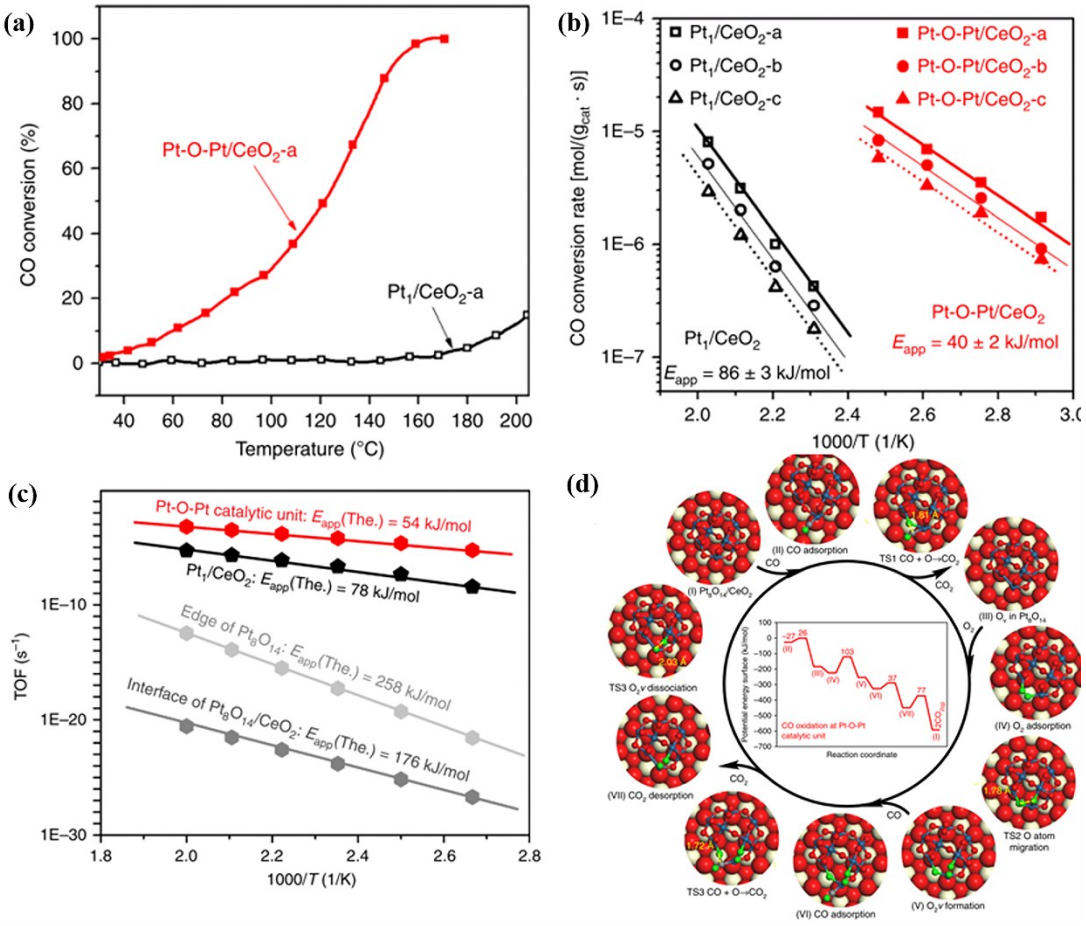

Figure 15. (a) CO oxidation light-off performance, (b) Active energies of CO oxidation rates, (c) Various CO oxidation routes on the Pt_1/ CeO_2 and Pt_8O_{14}/CeO_2 structures, and (d) Potential energy

diagrams and configurations for CO oxidation cycle over Pt-O-Pt/CeO_2.[188] Reprinted with permission from ref [188], Copyright 2019 Nature Publishing Group.

Wang et al. prepared an Ir-O-Ir structure of dinuclear heterogeneous catalysts (DHCs) on α-Fe_2O_3 by a facile photochemical method.[189] Significant performance, that was better than Ir SACs or Ir NPs, was measured on Ir DHCs in a water oxidation reaction. A mechanism for water oxidation on Ir DHC and Ir SACs was proposed, as shown in Figure 16. The first two steps were similar to those for Ir DHC and Ir SACs, both through proton-coupled electron transfer (PCET) steps twice. The main difference came from the third step. For Ir DHC, there was another PCET step before the formation of O–O bond, as shown in steps C to D in Figure 16a. For Ir SACs, it bound to a H_2O molecular and formed an O–O bond first before the third PCET (steps C to E), since direct oxidation of Ir SAC needed more than 1.8 eV of energy. In contrast, the presence of another Ir atom nearby in Ir DHC reduced the required energy to 1.2 eV. The results highlighted the synergistic effects between a dinuclear active center over a mononuclear active center. This work provided a convenient way to investigate the inherent mechanisms of heterogeneous catalysis involving multiple but individually separated active metal atoms, that contributed to the optimization of heterogeneous catalysts.

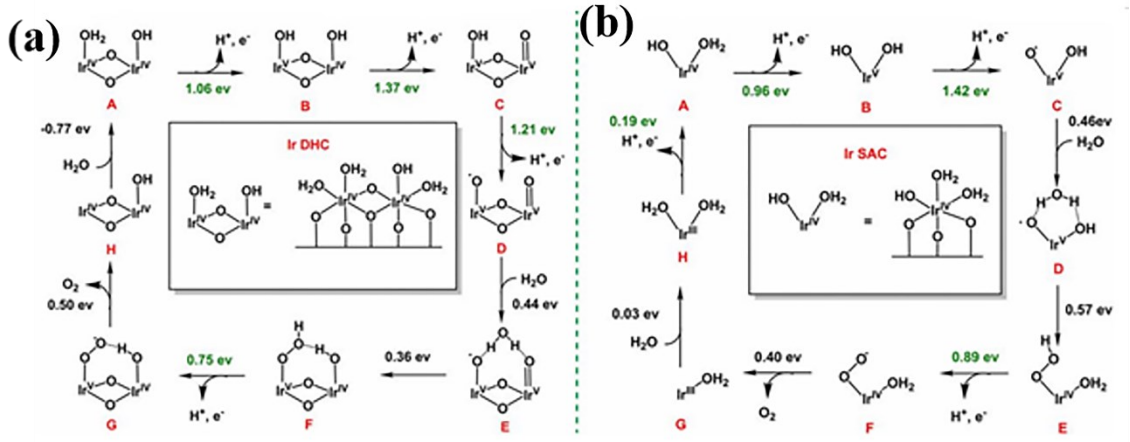

Figure 16. Proposed reaction pathway and DFT calculated reaction free energies at zero bias potential of (a) Ir DHC and (b) Ir SAC.[189] Reprinted with permission from ref [189], Copyright 2018 National Academy of Sciences.

Lu et al. prepared Pt_2 dimers, as well as Pt_1 single atoms, on a graphene support using ALD.[190] Pt_2 dimers, obtained by a second Pt ALD cycle, was deposited on Pt_1/graphene at 150 °C. The distances between the nearest Pt single atoms in the Pt_1/graphene were more than 2 nm, as confirmed by HAADF-STEM. However, Pt_2 dimers had a distance of 0.30±0.02 nm, which was significantly shorter than that in Pt_1/graphene. During the hydrolytic dehydrogenation of ammonia borane, Pt_2 dimers exhibited ~17- and 45-fold higher activity than Pt_1/graphene and Pt NPs, respectively. The superior performance for Pt_2 dimers resulted from weaker adsorption of ammonia borane on Pt_2 dimers, which had an adsorption energy of -2.81 eV, lower than that of Pt_1/graphene (-3.20 eV) and Pt NPs (-3.97 eV). Pt_2O_x was confirmed as the active center. The advantages of ALD made it possible to atomically deposit metal dimers on high-surface area supports.

4.2. Single atom with coordination atoms

Moreover, different metals can result in different active centers, even with the same support and identical synthesis method. Wang et al. used a porous N and S co-doped carbon framework to anchor Fe, Co, and Ni species to investigate different metal coordination environments and catalytic performance.[191] Using the same synthesis method, Fe SACs mainly consisted of a FeN_4S_2 ensemble, where S atoms formed bonds with the N atoms, as shown in Figure 17a. Co and Ni SACs preferred CoN_3S_1 and NiN_3S_1, where Co/Ni-S bonds formed. Fe species could only coordinate with the N atoms, whereas Ni and Co species could coordinate with both N and S. The coordination environment of S atoms was different. As for Fe SACs, the S atoms were mostly linked to neighboring C or N atoms, without Fe-S bonds. As for Co and Ni SACs, the S atoms partially replaced one N atom to form Co-S and Ni-S bonds, respectively. Different affinities of Fe and Co/Ni species towards the S-containing ligands resulted in different intermediates and, thus, different final structures[192]. In an ORR experiment, Fe SACs exhibited the highest performance, which was better than that of commercial Pt/C. The superior catalytic performance originated from the unique active centers. In Fe SACs, FeN_4S_2 acted as an active center. The electron easily transferred from S atoms to N atoms because of the relatively higher electronegativity of N. The resulted N atoms had a relatively negative charge, causing an increase of the electron density of Fe atoms. The increased electron density of Fe atoms led to an enhanced ORR activity. In contrast, the electron transferred from Co/Ni atoms to the S atoms, resulted in the inferior ORR performance

of Co and Ni SACs. DFT calculation also revealed that Fe SACs had the highest density states near the Fermi level, enhancing electron transfer for Fe SACs.

So far, it remains a major challenge to accurately adjust the coordination pattern of SACs at an atomic level. Much endeavor has been devoted to creating an exact active center.[125, 193-195] Zhang et al. prepared Fe SACs under different pyrolysis temperatures (600 ℃, 700 ℃, and 800 ℃), yielding four different types of FeN_x (x = 4–6) structures, which were identified by Mössbauer spectroscopy.[193] It was found that pyrolysis temperature had a critical effect on the distribution of Fe species. In selective oxidation of the C–H bond, Fe–N–C-700 exhibited the highest performance. Various catalytic performances originated from different active centers. For instance, D3 species, containing a N–($Fe^{III}N_4$)–N low-spin structure, were catalytically inert because of the saturated and strong coordination of the central Fe with six N atoms. D4 species, containing a N–($Fe^{III}N_4$) medium-spin structure, were the most catalytically active, as they had a larger amount of unsaturated coordination sites (Fe–N_5), as shown in Figure 17b. Meanwhile, the most active D4 species were the least abundant in Fe–N–C-700, indicating that it has the potential to promote performance by raising the number of D4 species.

A similar strategy was applied to fabricate Fe SACs with different Fe coordination environments.[12] In a benzene oxidation reaction (BOR), Fe SACs with Fe-N_4 sites exhibited the best BOR activity with 78.4% conversion of benzene and 100% selectivity of phenol, as shown in Figure 17c. However, the BOR performances of Fe SACs decreased gradually by one or two C atoms substituting the coordinating N atoms, suggesting a significant coordination sensitivity. DFT calculations revealed that the coordination environments influenced the formation of intermediates, thereby the reaction mechanism. Fe SACs with Fe-N_4 sites could adsorb and activate H_2O_2 to produce O=Fe=O effectively, which was a crucial intermediate for catalyzing BOR. The work provided a way to regulate the coordination pattern of SACs and enhance catalytic activity.

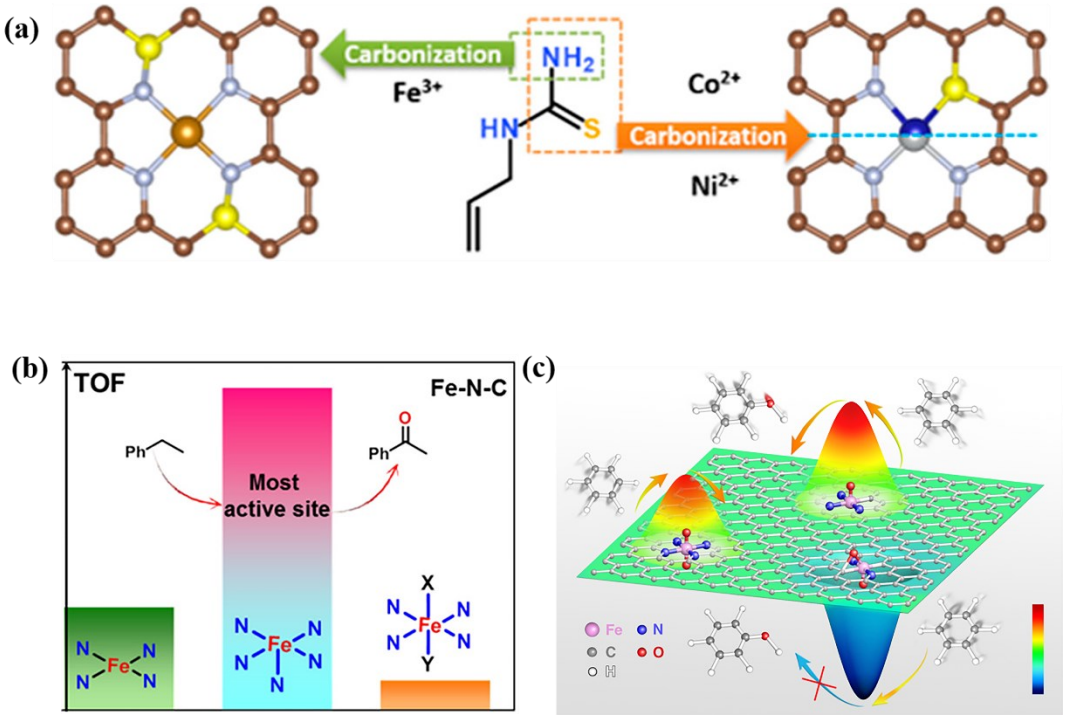

Figure 17. (a) Proposed structure of Fe, Co, and Ni SACs,[191] reprinted with permission from ref [191], Copyright 2019 American Chemical Society. (b) FeN_x species of Fe SACs,[193] reprinted with permission from ref [193], Copyright 2017 American Chemical Society. (c) The coordination effect of Fe SACs for benzene oxidation,[12] reprinted with permission from ref [12], Copyright 2019 Nature Publishing Group.

Jiang et al. prepared Ni SACs by a host-guest cooperative protection strategy.[194] The introduction of Mg^{2+} in MgNi-MOF-74 extended the spatial distance of adjacent Ni atoms, while the introduction of polypyrrole provided N source to stable Ni single atoms during high temperature decomposition. Ni SACs, with well controlled Ni-N coordination numbers, were obtained by varying the pyrolysis temperature from 600 ℃ to 800 ℃. The obtained Ni-N_2-C, with the lowest N coordination number, outperformed Ni-N_3-C and Ni-N_4-C with higher N coordination numbers in a CO_2 reduction reaction. The rate determining step for this reaction was the formation of COOH* intermediates for all of the Ni-N*x*-C. DFT calculation revealed that the required free energy charge of the rate determining step for Ni-N_2-C was 1.42 eV, which was lower than those of Ni-N_3-C (1.45 eV) and Ni-N_4-C (1.73 eV). Moreover, Ni-N_2-C had a much lower desorption energy for the formation of CO* than those of Ni-N_3-C and Ni-N_4-C, indicating easy release of

CO^* from Ni-N_2-C for CO production. With the same method, Fe and Co SACs, with controlled coordination numbers, were synthesized, demonstrating its universality.

Pennycook et al. fabricated Cu SACs with different types of Cu–N/C bonds for a nitrogen reduction reaction, and they identified Cu–N_2,[196] rather than Cu–N_4/N_3C,[197] as the efficient active center. EXAFS confirmed a mixture of Cu–N_2 and Cu–N_4/N_3C structure with weight percentages of 20% ± 5% and 80% ± 5%, respectively. DFT calculation showed a weak connection between N_2 and the center Cu atoms of Cu—N_4/N_3C, indicating a failure to activate the inert N≡N triple bond, hence impeding the subsequent nitrogen reduction reaction. In contrast, the Cu single atoms in a Cu–N_2 configuration strongly interacted with N_2. Although only 20% of the Cu–N_2 configuration existed, the atomized Cu SACs provided enough active centers for efficiently catalyzing the nitrogen reduction reaction. Yao et al. also confirmed Cu-N_2 as the active center for enhanced ORR performance via a $4e^-$ mechanistic pathway.[198] Because previous work only contained around 20% of Cu-N_2, future work should focus on how to increase the composition of Cu–N_2 configuration by adjusting experimental parameters.

4.3. Single atom with ligands and supports

Ligands play a critical role in the catalytic process. For example, metal hydrides are necessary for C–H bond activation, as well as for chain walking,[199] whereas a metal carbene is essential for olefin metathesis.[200] In some reactions, the real active center comprises single metal atoms with functional ligands, as well as well-defined surfaces.[201-202] The ligand may control the oxidation state, geometry, and d^n electron configuration of the metal center,[202] contributing significantly to the activity, selectivity, and stability of catalysts.[203-209] Depending on the ligands and supports attached to the center metal, the performance of prepared SACs may vary substantially.[210-211] Taking Pt SACs as an example, powdered MgO, Al_2O_3, and CeO_2 were used as supports to anchor a Pt single atom with a ligand 3,6-di-2-pyridyl-1,2,4,5tetrazine (DPTZ).[212] The nitrogen bidentate binding pockets in DPTZ can coordinate Pt and prevent aggregation, owing to its electron-accepting capability of stabilizing a non-zero oxidation state Pt.[213] The Pt-DPTZ SACs were synthesized by impregnating DPTZ and Pt precursor $H_2PtCl_6 \cdot 6H_2O$ on different supports in one step. The Pt oxidation was different in Pt/MgO SACs (+4 oxidation state) and Pt-DPTZ/MgO SACs (+2 oxidation state), due to the electron-accepting capability of DPTZ. Besides, DPTZ prevented the formation of Mg_2PtO_4 by coordinating with and stabilizing Pt. The DPTZ loading

on different supports was different because of different ligand-support interaction. The highest DPTZ loading of 94% was obtained on MgO because the basic oxygen on the surface of MgO easily reacted with the acidic tetrazine rings of DPTZ.[214] In contrast, only 0.41 and 0.42 of DPTZ loading was achieved on Al_2O_3 and CeO_2, respectively. The higher DPTZ loading facilitated the stabilization of Pt single atoms and, thus, Pt-DPTZ/MgO SACs showed the best performance in a hydrosilylation reaction between 1-octene and dimethoxymethysilane.

In the following research, the same group investigated the impact of ligands on Pt activity.[215] DPTZ, PDO(1,10-phenanthroline-4,7-ketone), and BMTZ (bis-pyrimidyltetrazine) ligands were used to prepare Pt SACs on MgO. The Pt valence state in Pt-DPTZ/MgO and Pt-PDO/MgO SACs was +2 oxidation state, while that in Pt-BMTZ/MgO SACs was +3 oxidation state, due to the stronger electron affinity of BMTZ. In a hydrosilylation reaction between 4-vinyl-1-cyclohexane 1,2-epoxide and trimethoxysilane, Pt-DPTZ/MgO and Pt-PDO/MgO SACs exhibited high performance, whereas Pt-BMTZ/MgO SACs showed no activity, since the activity of Pt in this reaction was highly sensitive to the electronic structure, which can be adjusted by the ligands. More research regarding the impact of ligands and supports can be found [202, 207, 216-219] as the sensitivity of the center metal to the local coordination environment is crucial for catalytic performance.

Above all, the activity of SACs was sensitive to the supports and ligands. It may come from the tuning of the electronic structure of metal centers as well as the distribution of metal atoms on supports. The SACs, serving as a prototype, provide vast potentials for the fine tuning of metal-ligand-support interaction.

4.4. Single-atom alloys (SAAs)

The compositions of SAAs include catalytically active metals atomically dispersed on a more inert metal.[220] The well-defined nature of the active centers in SAAs benefits the understanding of fundamental surface processes.[221] SAAs, prepared by the introduction of neighbor metals to decorate SACs, offer an efficient pathway to tailor the catalytic activity of SACs.[222-225] For instance, a specific rate of 12,000 mol_{H2} $mol_{Pt}^{-1}min^{-1}$ for the hydrolytic dehydrogenation of ammonia borane, at room temperature, was achieved by a Pt-Ni SAA.[226] The outstanding performance stemmed from the synergistic effect between Pt and Ni. In the Pt-Ni SAA, Pt had a negative charge ($Pt^{\delta-}$), while Ni had a positive charge ($Ni^{\delta+}$). Thus, Pt was prone to react with H of

H_2O molecules, whereas Ni preferred to react with OH of H_2O molecules. DFT was used to identify the catalytic mechanism. The kinetic barrier for the activation of H_2O molecules over Pt-Ni SAA and Ni sites on a pristine Ni surface were 0.75 eV and 0.88 eV, respectively. Thus, the individual Pt atom, surrounded by Ni atoms, acted as the active center, giving rise to an energetically favorable pathway. Flytzani-Stephanopoulos et al. also applied SAA strategy to Pt SACs, reducing the binding strength of CO, since Pt was notorious for its easy poisoning by strong CO adsorption.[227] As for Pt-Cu SAA, Pt single atoms were enclosed in the surface of Cu. The obtained $Pt_{0.008}$Cu-SAA exhibited the weakest Pt-CO bonds, whereas Pt NPs exhibited the strongest Pt-CO bonds. Therefore, more CO-free Pt sites were available, when CO appeared in the gas phase, enhancing the activity.

Isolated platinum atom geometries are inert for C–C bond scission, which leads to poor selectivity and activity. However, Sykes et al. found that Pt-Cu SAA provided excellent activity and selectivity in a butadiene hydrogenation reaction even under mild conditions.[64] In this study, CO was used to selectively cover Pt sites to determine the active centers for butadiene hydrogenation. The results indicated that butadiene hydrogenation was not affected by the introduction of CO, meaning that the isolated Pt facilitated the activation of H_2, and Cu sites which were responsible for hydrogenation. Therefore, isolated platinum atoms on Pt-Cu SAA became active for C-C bond scission. Besides, Pt-Cu SAA did not contain other Pt ensembles, where unfavorable reactions occurred. Thus, Pt-Cu SAA inhabited hydrocarbon decomposition, which was commonly observed with Pt catalysts, leading to high selectivity.

SAAs exhibited geometric and electronic structures that were different from those of the single atoms that were prepared by anchoring on the support.[228] The SAA approach offers huge advantages of synergistic catalysis between isolated atoms and a host metal, including improved activity and selectivity and resistance to CO poisoning. So far, most reports have focused on a combination of trace amounts of group 8~10 transition metals (e.g., Pd, Pt, Rh, Ni, and Ru) alloyed into group XI metals (e.g., Cu, Ag, and Au). More combinations should be explored.

4.5. Metal-support interactions

Strong metal-support interactions can cause mass transport and charge transfer between supports and metals, thus significantly improving the activity and stability of catalysts.[229] Murray et al. investigated the interactions between CeO_2 and supported metals (Ni, Pd, and Pt nanocrystals)

through CO oxidation, and they found that metal-support interface sites played a vital role in enhanced catalytic performance.[230] The metal-support interactions are more important for SACs than for their NP counterparts, due to higher surface free energy.[4] The supports may be directly involved in the reaction. Taking CO oxidation as an example, Pt_1/FeO_x exhibited excellent activities,[20] while Pt_1/SiO_2 showed no activity, even at a higher temperature.[58] To this end, it is vital to investigate and determine how the supports interact with single atoms.

Zheng et al. prepared Pd_1/TiO_2 SACs with Ti (III) vicinal to Pd to investigate the metal-support interactions.[231] Fresh prepared Pd_1/TiO_2-EG (ethylene glycolate) went through a thermal treatment at 350 ℃ for various durations to obtain different amounts of exposed Ti (III)-O-Pd interfaces. In the CO oxidation, the sample with more Ti (III)-O-Pd interfaces had a better activity. Kinetic analysis confirmed that O_2 activation, rather than CO adsorption, was the rate-limiting step. X-band electron spin resonance (ESR) identified that the exposed Ti (III)-O-Pd interfaces could activate O_2 into O_2^-. The O_2^- species easily reacted with CO at the Ti (III)-O-Pd interfaces, even at room temperature. DFT calculations proposed the binding of structures of O_2 adsorbed at the Ti (III)-O-Pd interfaces. The bridging structure in Figure 18a had the lowest adsorption energy. The reaction mechanism on how the Ti(III)-O-Pd interfaces promoted CO oxidation was demonstrated by DFT calculations, as shown in Figure 18d. The reaction went through TS1 path after CO and O_2 co-adsorbed at the Ti (III)-O-Pd interfaces, with a barrier of 0.16 eV. After this, one O atom still remained on the Ti (III)-O-Pd interfaces, which also exhibited high activity with a small barrier of 0.22 eV. Combining a DFT calculation with experiment results, the authors confirmed that the real active center was the Ti (III)-O-Pd interfaces.

Zhang et al. also investigated the role of metal-support interface by preparing Pd SACs on Co_xO_y nanoarrays with tunable facets.[232] Different Pd-Co_xO_y interfaces were obtained due to the convertible cobalt supports with specific facets. The surface chemical state of Co_xO_y nanoarrays was essential in promoting catalytic activity. Pd atoms anchored on the high-index (112) facet of cobalt support exhibited the best performance in CO oxidation. Oxygen vacancies on the high-index (112) facet were preferential sites for the adsorption of Pd atoms. The formation of Pd-O-Co was critical for the activity and stability of the obtained Pd SACs. Moreover, Mpourmpakis et al. used DFT to investigate the metal−support interactions of a series of transition-metal atoms supported on three common oxide supports (i.e., γ-Al_2O_3, MgO, and $MgAl_2O_4$).[233] A predictable

model for the strength of metal−support interactions was developed, guiding the design of stable SACs.

From these studies, we can see that the real active center for SACs can be far beyond isolated metal atoms themselves.[231] Supports are sometimes involved in the reactions, especially for reducible metal oxide. SACs serve as a good model to design high activity catalysts by precisely controlling metal-support interfaces. DFT is a powerful tool to rationalize experimental observations, elucidate the underlying physics of the metal-support interactions, and guide experiments for the synthesis of stable SACs.

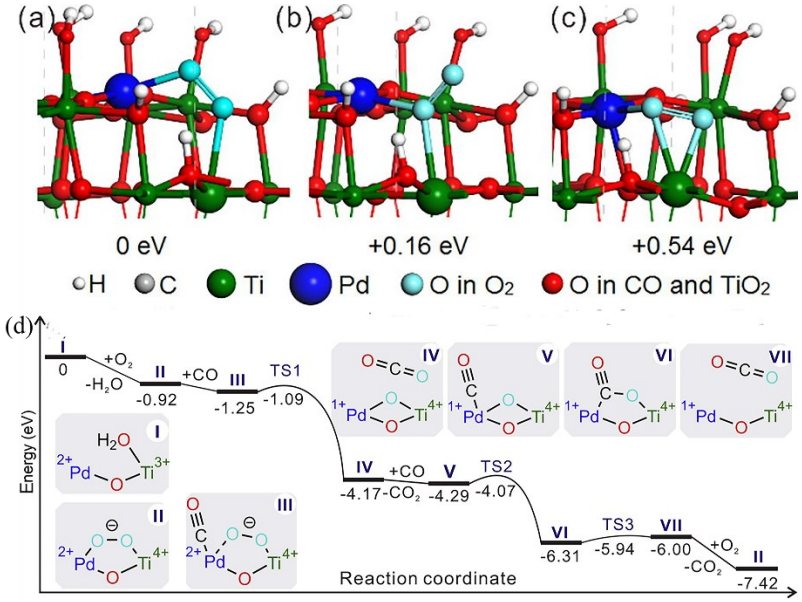

Figure 18. Possible binding structures of O_2 adsorbed at the Ti (III)-O-Pd interfaces: (a) bridging structure, (b) the end-on configuration, and (c) the side-on configuration. (d) Possible reaction mechanism of CO oxidation at the Ti (III)-O-Pd(II) interface.[231] Reprinted with permission from ref [231], Copyright 2018 Elsevier Inc.

5. Summary and Outlook

In this review, the recent development of high metal loading (>5 wt.%) SACs has been summarized and discussed. A focus has been on systematically reviewing appropriate substrates, characterization techniques, and active centers. A well-designed substrate is crucial for the preparation of high metal loading SACs. With the assistance of advanced characterization techniques, direct observation of SACs can be achieved. By fabricating a suitable active center,

the obtained SACs can surpass the single-atom catalytic activity limit. However, great challenges still need to be tackled in the SACs field. These include:

(1) Large scale synthesis of high metal loading SACs: It is highly desirable to scale up the synthesis of high metal loading SACs to meet practical applications. Large-scale preparation of heteroatom-doped substrates is essential, and novel synthesis strategies should be explored. Theoretical calculations and modeling need to be further developed to guide the scale-up synthesis.

(2) Structural characterizations: More efforts should be devoted to fully understanding the 3D distribution of SACs. *In situ* characterization techniques need to be explored for more reactions, with the development of the sample holder, image reconstruction algorithms and equipment resolution. A facile method for full characterization of SACs is extremely welcome since some existing equipment resources are still scarce and expensive.

(3) Diversity of the substrates: The substrates used for the synthesis of high metal loading SACs are mainly confined to carbon-based materials, due to the easy introduction of N, S, and O atoms. One big issue of carbon-based materials is poor thermal stability at high temperatures, especially in an oxygen atmosphere. The limitation of substrates also limits the application of SACs. Most of the reported reactions catalyzed by high metal loading SACs are electrochemical reactions, because of mild reaction conditions. It would be beneficial to apply high metal loading SACs to other various catalysis fields if the substrates are more diversified. Metal oxide is a good candidate, owing to its high thermal stability and conductivity. Few researchers are studying the synthesis of SACs on metal oxides. Recently, our group reported Fe single atoms deposited on various metal oxide substrates including multi-walled carbon tubes, TiO_2, and SiO_2 by ALD, but the loading of Fe single atoms was up to 2 wt.%.[36] ALD could be a good approach to deposit single atoms on various metal oxides. Still, great endeavor should be devoted to exploring the choice of the substrates and pre-treatment of supports before loading of SACs, thus enlarging the applications of the high metal loading SACs.

(4) Construction of suitable active center: A well-designed structure of SACs facilitates the investigation of the complicated heterogeneous catalytic reactions at the atomic scale. Combining advanced characterization techniques with theoretical calculation, the active center can be confirmed. However, most research only focuses on metal species. Attention should also be given to the role of substrates, since the interaction between single metal atoms and the substrates also contributes greatly to catalytic performance. Moreover, it is highly desirable to adjust the

coordination pattern of metal atoms precisely, which can significantly improve the catalytic activity of SACs.

(5) Reactions under practical conditions: Most of the reactions catalyzed by SACs occur under ideal conditions, using modeling sources. SACs may exhibit excellent performance under these conditions. However, impurities or poisonous materials usually exist in practical applications, and side reactions could exist, undermining selectivity. The adverse impacts of these impurities or poisonous materials on SACs may be more serious than that on NPs. Therefore, it is necessary to conduct reactions under real conditions, and to promote the utilizations of SACs in practical applications.

(6) Broaden applications: Currently, the applications of SACs mainly focus on energy related reactions, such as CO_2 conversion to fuels and electrochemical conversion nitrogen to ammonia. More fields should be explored in order to use SACs to obtain better performance. One promising field is the usage of SACs in the sensor field. Sensors made from SACs have shown higher selectivity and sensitivity, shorter response time, and longer lifetime than those made from NPs.[234-235] Moreover, single atom nanozymes have exhibited similar biocatalytic performance under harsh conditions, compared to their natural counterparts. Still, the application of SACs is in infancy. Continuous efforts should be devoted to broadening the applications of SACs.

Acknowledgements

This work was supported in part by the National Science Foundation Grant NSF 1803812.

Keywords: Active center analysis; High metal loading; *In situ* characterization; Single-atom catalysts; Synthesis strategies.

References

[1] H. Fei, J. Dong, M. J. Arellano-Jimenez, G. Ye, N. Dong Kim, E. L. Samuel, Z. Peng, Z. Zhu, F. Qin, J. Bao, M. J. Yacaman, P. M. Ajayan, D. Chen, J. M. Tour, *Nat. Commun.* **2015**, *6*, 8668.

[2] M. Moliner, J. E. Gabay, C. E. Kliewer, R. T. Carr, J. Guzman, G. L. Casty, P. Serna, A. Corma, *J. Am. Chem. Soc.* **2016**, *138*, 15743-15750.

[3] J. Li, H. Huang, P. Liu, X. Song, D. Mei, Y. Tang, X. Wang, C. Zhong, *J. Catal.* **2019**, *375*, 351-360.

[4] J. Li, Q. Guan, H. Wu, W. Liu, Y. Lin, Z. Sun, X. Ye, X. Zheng, H. Pan, J. Zhu, S. Chen, W. Zhang, S. Wei, J. Lu, *J. Am. Chem. Soc.* **2019**, *141*, 14515-14519.
[5] M. Li, K. Duanmu, C. Wan, T. Cheng, L. Zhang, S. Dai, W. Chen, Z. Zhao, P. Li, H. Fei, Y. Zhu, R. Yu, J. Luo, K. Zang, Z. Lin, M. Ding, J. Huang, H. Sun, J. Guo, X. Pan, W. A. Goddard, P. Sautet, Y. Huang, X. Duan, *Nat. Catal.* **2019**, *2*, 495-503.
[6] L. Lin, S. Yao, R. Gao, X. Liang, Q. Yu, Y. Deng, J. Liu, M. Peng, Z. Jiang, S. Li, Y. W. Li, X. D. Wen, W. Zhou, D. Ma, *Nat. Nanotechnol.* **2019**, *14*, 354-361.
[7] D. Liu, X. Li, S. Chen, H. Yan, C. Wang, C. Wu, Y. A. Haleem, S. Duan, J. Lu, B. Ge, P. M. Ajayan, Y. Luo, J. Jiang, L. Song, *Nat. Energy* **2019**, *4*, 512-518.
[8] J. Liu, M. Jiao, B. Mei, Y. Tong, Y. Li, M. Ruan, P. Song, G. Sun, L. Jiang, Y. Wang, Z. Jiang, L. Gu, Z. Zhou, W. Xu, *Angew. Chem. Int. Ed.* **2019**, *58*, 1163-1167.
[9] X. Lv, W. Wei, P. Zhao, D. Er, B. Huang, Y. Dai, T. Jacob, *J. Catal.* **2019**, *378*, 97-103.
[10] M. Melchionna, P. Fornasiero, *Chem* **2019**, *5*, 1927-1928.
[11] L. Nie, D. Mei, H. Xiong, B. Peng, Z. Ren, X. I. P. Hernandez, A. DeLaRiva, M. Wang, M. H. Engelhard, L. Kovarik, A. K. Datye, Y. Wang, *Science* **2017**, *358*, 1419-1423.
[12] Y. Pan, Y. Chen, K. Wu, Z. Chen, S. Liu, X. Cao, W. C. Cheong, T. Meng, J. Luo, L. Zheng, C. Liu, D. Wang, Q. Peng, J. Li, C. Chen, *Nat. Commun.* **2019**, *10*, 4290.
[13] J. Park, S. Lee, H. E. Kim, A. Cho, S. Kim, Y. Ye, J. W. Han, H. Lee, J. H. Jang, J. Lee, *Angew. Chem. Int. Ed.* **2019**, *131*, 16184-16188.
[14] X. I. Pereira-Hernandez, A. DeLaRiva, V. Muravev, D. Kunwar, H. Xiong, B. Sudduth, M. Engelhard, L. Kovarik, E. J. M. Hensen, Y. Wang, A. K. Datye, *Nat. Commun.* **2019**, *10*, 1358.
[15] S. Shin, J. Kim, S. Park, H. E. Kim, Y. E. Sung, H. Lee, *Chem. Commun.* **2019**, *55*, 6389-6392.
[16] T. Maschmeyer, F. Rey, G. Sankar, J. M. Thomas, *Nature* **1995**, *378*, 159-162.
[17] D. V. Yandulov, R. R. Schrock, *Science* **2003**, *301*, 76-78.
[18] Q. Fu, H. Saltsburg, M. Flytzani-Stephanopoulos, *Science* **2003**, *301*, 935-938.
[19] X. Zhang, H. Shi, B.-Q. Xu, *Angew. Chem. Int. Ed.* **2005**, *117*, 7294-7297.
[20] B. Qiao, A. Wang, X. Yang, L. F. Allard, Z. Jiang, Y. Cui, J. Liu, J. Li, T. Zhang, *Nat. Chem.* **2011**, *3*, 634-641.
[21] J. D. Benck, T. R. Hellstern, J. Kibsgaard, P. Chakthranont, T. F. Jaramillo, *ACS Catal.* **2014**, *4*, 3957-3971.
[22] Z. W. Seh, J. Kibsgaard, C. F. Dickens, I. Chorkendorff, J. K. Norskov, T. F. Jaramillo, *Science* **2017**, *355*, eaad4998.
[23] H. Li, L. Wang, Y. Dai, Z. Pu, Z. Lao, Y. Chen, M. Wang, X. Zheng, J. Zhu, W. Zhang, R. Si, C. Ma, J. Zeng, *Nat. Nanotechnol.* **2018**, *13*, 411-417.
[24] R. Qin, K. Liu, Q. Wu, N. Zheng, *Chem. Rev.* **2020**. https://doi.org/10.1021/acs.chemrev.0c00094
[25] J. Xing, J. F. Chen, Y. H. Li, W. T. Yuan, Y. Zhou, L. R. Zheng, H. F. Wang, P. Hu, Y. Wang, H. J. Zhao, Y. Wang, H. G. Yang, *Chemistry* **2014**, *20*, 2138-2144.
[26] H. Wei, X. Liu, A. Wang, L. Zhang, B. Qiao, X. Yang, Y. Huang, S. Miao, J. Liu, T. Zhang, *Nat. Commun.* **2014**, *5*, 5634.
[27] J. Wang, Z. Li, Y. Wu, Y. Li, *Adv. Mater.* **2018**, *30*, e1801649.
[28] A. Wang, J. Li, T. Zhang, *Nat. Rev. Chem.* **2018**, *2*, 65-81.
[29] Y. W. C. Wang, J. Ge, Z. Xie, *Chem* **2019**, *5*, 2736-2737.
[30] Q. K. Li, X. F. Li, G. Zhang, J. Jiang, *J. Am. Chem. Soc.* **2018**, *140*, 15149-15152.
[31] D. A. Reed, B. K. Keitz, J. Oktawiec, J. A. Mason, T. Runcevski, D. J. Xiao, L. E. Darago, V. Crocella, S. Bordiga, J. R. Long, *Nature* **2017**, *550*, 96-100.
[32] M. Dhiman, V. Polshettiwar, *ChemCatChem* **2018**, *10*, 881-906.
[33] B. Han, R. Lang, B. Qiao, A. Wang, T. Zhang, *Chin. J. Catal.* **2017**, *38*, 1498–1507.
[34] X. Li, X. Yang, Y. Huang, T. Zhang, B. Liu, *Adv. Mater.* **2019**, *31*, e1902031.
[35] J. Liu, B. R. Bunes, L. Zang, C. Wang, *Environ. Chem. Lett.* **2017**, *16*, 477-505.
[36] X. Wang, B. Jin, X. He, T. A. White, X. Liang, *Catal. Lett.* **2020**, *94*, 237–244.
[37] X. Wang, B. Jin, Y. Jin, T. Wu, L. Ma, X. Liang, *ACS Applied Nano Materials* **2020**, *3*, 2867-2874.

[38] P. Hu, Z. Huang, Z. Amghouz, M. Makkee, F. Xu, F. Kapteijn, A. Dikhtiarenko, Y. Chen, X. Gu, X. Tang, *Angew. Chem. Int. Ed.* **2014**, *53*, 3418-3421.
[39] J. Liang, X. Yang, C. Xu, T. Zhang, J. Li, *Chin. J. Catal.* **2017**, *38*, 1566-1573.
[40] X. Guo, G. Fang, G. Li, H. Ma, H. Fan, L. Yu, C. Ma, X. Wu, D. Deng, M. Wei, D. Tan, R. Si, S. Zhang, J. Li, L. Sun, Z. Tang, X. Pan, X. Bao, *Science* **2014**, *344*, 616-619.
[41] G. Kwon, G. A. Ferguson, C. J. Heard, E. C. Tyo, C. Yin, J. DeBartolo, S. Seifert, R. E. Winans, A. J. Kropf, J. Greeley, R. L. Johnston, L. A. Curtiss, M. J. Pellin, S. Vajda, *ACS Nano* **2013**, *7*, 5808-5817.
[42] C. Asokan, L. DeRita, P. Christopher, *Chin. J. Catal.* **2017**, *38*, 1473-1480.
[43] X. Li, X. Yang, J. Zhang, Y. Huang, B. Liu, *ACS Catal.* **2019**, *9*, 2521-2531.
[44] J. Liu, *Chin. J. Catal.* **2017**, *38*, 1460-1472.
[45] I. Ogino, *Chin. J. Catal.* **2017**, *38*, 1481-1488.
[46] J. Liu, *ACS Catal.* **2016**, *7*, 34-59.
[47] M. Flytzani-Stephanopoulos, *Chin. J. Catal.* **2017**, *38*, 1432-1442.
[48] L. Wang, L. Huang, F. Liang, S. Liu, Y. Wang, H. Zhang, *Chin. J. Catal.* **2017**, *38*, 1528-1539.
[49] Y. Chen, S. Ji, C. Chen, Q. Peng, D. Wang, Y. Li, *Joule* **2018**, *2*, 1242-1264.
[50] H. Yan, C. Su, J. He, W. Chen, *J. Mater. Chem. A* **2018**, *6*, 8793-8814.
[51] L. Zhang, Y. Ren, W. Liu, A. Wang, T. Zhang, *Natl. Sci. Rev.* **2018**, *5*, 653-672.
[52] H. Fei, J. Dong, D. Chen, T. Hu, X. Duan, I. Shakir, Y. Huang, X. Duan, *Chem. Soc. Rev.* **2019**, *48*, 5207-5241.
[53] Q. Liu, Z. Zhang, *Catal. Sci. Technol.* **2019**, *9*, 4821-4834.
[54] X. Li, Z. Yuan, J. Meng, Z. Li, S. He, *J. Phys. Chem. C* **2015**, *119*, 15414-15420.
[55] C. Doornkamp, V. Ponec, *J. Mater. Chem. A* **2000**, *162*, 19-32.
[56] A. J. Therrien, A. J. R. Hensley, M. D. Marcinkowski, R. Zhang, F. R. Lucci, B. Coughlin, A. C. Schilling, J. McEwen, E. C. H. Sykes, *Nat. Catal.* **2018**, *1*, 192–198.
[57] R. Bliem, J. E. S. van der Hoeven, J. Hulva, J. Pavelec, O. Gamba, P. E. d. Jongh, M. Schmid, P. Blaha, U. Diebold, G. S. Parkinson, *Proc. Natl. Acad. Sci. U. S. A.* **2016**, *113*, 8921–8926.
[58] K. Ding, A. Gulec, A. M. Johnson, N. M. Schweitzer, G. D. Stucky, L. D. Marks, P. C. Stair, *Science* **2015**, *350*, 189-192.
[59] J. D. Kistler, N. Chotigkrai, P. Xu, B. Enderle, P. Praserthdam, C. Y. Chen, N. D. Browning, B. C. Gates, *Angew. Chem. Int. Ed.* **2014**, *53*, 8904-8907.
[60] M. Moses-DeBusk, M. Yoon, L. F. Allard, D. R. Mullins, Z. Wu, X. Yang, G. Veith, G. M. Stocks, C. K. Narula, *J. Am. Chem. Soc.* **2013**, *135*, 12634-12645.
[61] C. Wang, X.-K. Gu, H. Yan, Y. Lin, J. Li, D. Liu, W. Li, J. Lu, *ACS Catal.* **2017**, *7*, 887–891.
[62] B. Zhang, H. Asakura, J. Zhang, J. Zhang, S. De, N. Yan, *Angew. Chem. Int. Ed.* **2016**, *55*, 8319-8323.
[63] J. Zhang, Z. Gao, S. Wang, G. Wang, X. Gao, B. Zhang, S. Xing, S. Zhao, Y. Qin, *Nat. Commun.* **2019**, *10*, 4166.
[64] F. R. Lucci, J. Liu, M. D. Marcinkowski, M. Yang, L. F. Allard, M. Flytzani-Stephanopoulos, E. C. Sykes, *Nat. Commun.* **2015**, *6*, 8550.
[65] Y. Ma, B. Chi, W. Liu, L. Cao, Y. Lin, X. Zhang, X. Ye, S. Wei, J. Lu, *ACS Catal.* **2019**, *9*, 8404-8412.
[66] H. Wei, Y. Ren, A. Wang, X. Liu, X. Liu, L. Zhang, S. Miao, L. Li, J. Liu, J. Wang, G. Wang, D. Su, T. Zhang, *Chem. Sci.* **2017**, *8*, 5126-5131.
[67] P. L. Gai, K. Yoshida, M. R. Ward, M. Walsh, R. T. Baker, L. van de Water, M. J. Watson, E. D. Boyes, *Catal. Sci. Technol.* **2016**, *6*, 2214-2227.
[68] D. Pierre, W. Deng, M. Flytzani-Stephanopoulos, *Top. Catal.* **2007**, *46*, 363-373.
[69] M. Yang, J. Liu, S. Lee, B. Zugic, J. Huang, L. F. Allard, M. Flytzani-Stephanopoulos, *J. Am. Chem. Soc.* **2015**, *137*, 3470-3473.
[70] Y. Zhai, D. Pierre, R. Si, W. Deng, P. Ferrin, A. U. Nilekar, G. Peng, J. A. Herron, D. C. Bell, H. Saltsburg, M. Mavrikakis, M. Flytzani-Stephanopoulos, *Science* **2010**, *329*, 1633-1636.

[71] B. Zugic, D. C. Bell, M. Flytzani-Stephanopoulos, *Appl. Catal., B* **2014**, *144*, 243-251.
[72] S. Yang, J. Kim, Y. J. Tak, A. Soon, H. Lee, *Angew. Chem. Int. Ed.* **2016**, *55*, 2058-2062.
[73] J. Liu, M. Jiao, L. Lu, H. M. Barkholtz, Y. Li, Y. Wang, L. Jiang, Z. Wu, D. J. Liu, L. Zhuang, C. Ma, J. Zeng, B. Zhang, D. Su, P. Song, W. Xing, W. Xu, Y. Wang, Z. Jiang, G. Sun, *Nat. Commun.* **2017**, *8*, 15938.
[74] X. Fang, Q. Shang, Y. Wang, L. Jiao, T. Yao, Y. Li, Q. Zhang, Y. Luo, H. L. Jiang, *Adv. Mater.* **2018**, *30*, 1705112.
[75] Y. Feng, Y. Guan, H. Zhang, Z. Huang, J. Li, Z. Jiang, X. Gu, Y. Wang, *J. Mater. Chem. A* **2018**, *6*, 11783-11789.
[76] J. Kim, C.-W. Roh, S. K. Sahoo, S. Yang, J. Bae, J. W. Han, H. Lee, *Adv. Energy Mater.* **2018**, *8*, 1701476.
[77] X. Zeng, J. Shui, X. Liu, Q. Liu, Y. Li, J. Shang, L. Zheng, R. Yu, *Adv. Energy Mater.* **2018**, *8*, 1701345.
[78] L. Zhang, J. Fischer, Y. Jia, X. Yan, W. Xu, X. Wang, J. Chen, D. Yang, H. Liu, L. Zhuang, M. Hankel, D. J. Searles, K. Huang, S. Feng, C. L. Brown, X. Yao, *J. Am. Chem. Soc.* **2018**, *140*, 10757-10763.
[79] K. Chi, Z. Chen, F. Xiao, W. Guo, W. Xi, J. Liu, H. Yan, Z. Zhang, J. Xiao, J. Liu, J. Luo, S. Wang, K. P. Loh, *J. Mater. Chem. A* **2019**, *7*, 15575-15579.
[80] K. Jiang, B. Liu, M. Luo, S. Ning, M. Peng, Y. Zhao, Y. R. Lu, T. S. Chan, F. M. F. de Groot, Y. Tan, *Nat. Commun.* **2019**, *10*, 1743.
[81] W. H. Lai, L. F. Zhang, W. B. Hua, S. Indris, Z. C. Yan, Z. Hu, B. Zhang, Y. Liu, L. Wang, M. Liu, R. Liu, Y. X. Wang, J. Z. Wang, Z. Hu, H. K. Liu, S. L. Chou, S. X. Dou, *Angew. Chem. Int. Ed.* **2019**, *58*, 11868-11873.
[82] F. Li, J. Baek, *Nat. Catal.* **2019**, *2*, 477–478.
[83] R. Shen, W. Chen, Q. Peng, S. Lu, L. Zheng, X. Cao, Y. Wang, W. Zhu, J. Zhang, Z. Zhuang, C. Chen, D. Wang, Y. Li, *Chem* **2019**, *5*, 2099-2110.
[84] X. Song, N. Li, H. Zhang, H. Wang, L. Wang, Z. Bian, *J. Power Sources* **2019**, *435*, 226771.
[85] S. Yang, Y. Yu, M. Dou, Z. Zhang, L. Dai, F. Wang, *Angew. Chem. Int. Ed.* **2019**, *131*, 14866-14872.
[86] H. Yin, S. Li, L. Gan, P. Wang, *J. Mater. Chem. A* **2019**, *7*, 11908-11914.
[87] B. Zhang, G. Sun, S. Ding, H. Asakura, J. Zhang, P. Sautet, N. Yan, *J. Am. Chem. Soc.* **2019**, *141*, 8185-8197.
[88] L. Zhang, K. Doyle-Davis, X. Sun, *Energy Environ. Sci.* **2019**, *12*, 492-517.
[89] Q. Zuo, T. Liu, C. Chen, Y. Ji, X. Gong, Y. Mai, Y. Zhou, *Angew. Chem. Int. Ed.* **2019**, *58*, 10198-10203.
[90] Z. Li, S. Ji, Y. Liu, X. Cao, S. Tian, Y. Chen, Z. Niu, Y. Li, *Chem. Rev.* **2020**, *120*, 623-682.
[91] S. An, G. Zhang, T. Wang, W. Zhang, K. Li, C. Song, J. T. Miller, S. Miao, J. Wang, X. Guo, *ACS Nano* **2018**, *12*, 9441-9450.
[92] H. Yan, X. Zhao, N. Guo, Z. Lyu, Y. Du, S. Xi, R. Guo, C. Chen, Z. Chen, W. Liu, C. Yao, J. Li, S. J. Pennycook, W. Chen, C. Su, C. Zhang, J. Lu, *Nat. Commun.* **2018**, *9*, 3197.
[93] S. Ji, Y. Chen, X. Wang, Z. Zhang, D. Wang, Y. Li, *Chem. Rev.* **2020**. https://doi.org/10.1021/acs.chemrev.9b00818
[94] P. Liu, Y. Zhao, R. Qin, S. Mo, G. Chen, L. Gu, D. M. Chevrier, P. Zhang, Q. Guo, D. Zang, B. Wu, G. Fu, N. Zheng, *Science* **2016**, *352*, 797-801.
[95] S. Cao, M. Yang, A. O. Elnabawy, A. Trimpalis, S. Li, C. Wang, F. Goltl, Z. Chen, J. Liu, J. Shan, M. Li, T. Haas, K. W. Chapman, S. Lee, L. F. Allard, M. Mavrikakis, M. Flytzani-Stephanopoulos, *Nat. Chem.* **2019**, *11*, 1098-1105.
[96] J. Wu, L. Xiong, B. Zhao, M. Liu, L. Huang, *Small Methods* **2019**, *4*, 1900540.
[97] Y. Li, J. Wu, B. Zhang, W. Wang, G. Zhang, Z. W. Seh, N. Zhang, J. Sun, L. Huang, J. Jiang, J. Zhou, Y. Sun, *Energy Storage Mater.* **2020**, *30*, 250-259.

[98] W. Liu, L. Zhang, W. Yan, X. Liu, X. Yang, S. Miao, W. Wang, A. Wang, T. Zhang, *Chem. Sci.* **2016**, *7*, 5758-5764.
[99] C. H. Choi, M. Kim, H. C. Kwon, S. J. Cho, S. Yun, H. T. Kim, K. J. Mayrhofer, H. Kim, M. Choi, *Nat. Commun.* **2016**, *7*, 10922.
[100] P. Yin, T. Yao, Y. Wu, L. Zheng, Y. Lin, W. Liu, H. Ju, J. Zhu, X. Hong, Z. Deng, G. Zhou, S. Wei, Y. Li, *Angew. Chem. Int. Ed.* **2016**, *55*, 10800-10805.
[101] C. Wang, H. Song, C. Yu, Z. Ullah, Z. Guan, R. Chu, Y. Zhang, L. Zhao, Q. Li, L. Liu, *J. Mater. Chem. A* **2020**, *8*, 3421-3430.
[102] Y. Chen, S. Ji, Y. Wang, J. Dong, W. Chen, Z. Li, R. Shen, L. Zheng, Z. Zhuang, D. Wang, Y. Li, *Angew. Chem. Int. Ed.* **2017**, *56*, 6937-6941.
[103] W. Liu, Y. Chen, H. Qi, L. Zhang, W. Yan, X. Liu, X. Yang, S. Miao, W. Wang, C. Liu, A. Wang, J. Li, T. Zhang, *Angew. Chem. Int. Ed.* **2018**, *57*, 7071-7075.
[104] D. Deng, X. Chen, L. Yu, X. Wu, Q. Liu, Y. Liu, H. Yang, H. Tian, Y. Hu, P. Du, R. Si, J. Wang, X. Cui, H. Li, J. Xiao, T. Xu, J. Deng, F. Yang, P. N. Duchesne, P. Zhang, J. Zhou, L. Sun, J. Li, X. Pan, X. Bao, *Sci. Adv.* **2015**, *1*, e1500462.
[105] L. Han, X. Liu, J. Chen, R. Lin, H. Liu, F. Lu, S. Bak, Z. Liang, S. Zhao, E. Stavitski, J. Luo, R. R. Adzic, H. L. Xin, *Angew. Chem. Int. Ed.* **2019**, *58*, 2321-2325.
[106] T. Li, J. Liu, Y. Song, F. Wang, *ACS Catal.* **2018**, *8*, 8450-8458.
[107] Z. Zhang, Y. Chen, L. Zhou, C. Chen, Z. Han, B. Zhang, Q. Wu, L. Yang, L. Du, Y. Bu, P. Wang, X. Wang, H. Yang, Z. Hu, *Nat. Commun.* **2019**, *10*, 1657.
[108] C. Rivera-Cárcamo, P. Serp, *ChemCatChem* **2018**, *10*, 5058-5091.
[109] G. Han, Y. Zheng, X. Zhang, Z. Wang, Y. Gong, C. Du, M. N. Banis, Y. Yiu, T. Sham, L. Gu, Y. Sun, Y. Wang, J. Wang, Y. Gao, G. Yin, X. Sun, *Nano Energy* **2019**, *66*, 104088.
[110] L. Zhao, Y. Zhang, L. B. Huang, X. Z. Liu, Q. H. Zhang, C. He, Z. Y. Wu, L. J. Zhang, J. Wu, W. Yang, L. Gu, J. S. Hu, L. J. Wan, *Nat. Commun.* **2019**, *10*, 1278.
[111] F. Li, G. Han, H. Noh, S. Kim, Y. Lu, H. Y. Jeong, Z. Fu, J. Baek, *Energy Environ. Sci.* **2018**, *11*, 2263-2269.
[112] J. Yi, R. Xu, G. Chai, T. Zhang, K. Zang, B. Nan, H. Lin, Y. Liang, J. Lv, J. Luo, R. Si, Y. Huang, R. Cao, *J. Mater. Chem. A* **2019**, *7*, 1252-1259.
[113] J. Yi, R. Xu, Q. Wu, T. Zhang, K. Zang, J. Luo, Y. Liang, Y. Huang, R. Cao, *ACS Energy Lett.* **2018**, *3*, 883-889.
[114] J. Li, S. Chen, N. Yang, M. Deng, S. Ibraheem, J. Deng, J. Li, L. Li, Z. Wei, *Angew. Chem. Int. Ed.* **2019**, *58*, 7035-7039.
[115] J. Zhao, Z. Chen, *J. Am. Chem. Soc.* **2017**, *139*, 12480-12487.
[116] H. Yang, L. Shang, Q. Zhang, R. Shi, G. I. N. Waterhouse, L. Gu, T. Zhang, *Nat. Commun.* **2019**, *10*, 4585.
[117] G. Chen, S. Neupane, W. Li, L. Chen, J. Zhang, *Carbon* **2013**, *52*, 468-475.
[118] S. Zhao, Y. Cheng, J. Veder, B. Johannessen, M. Saunders, L. Zhang, C. Liu, M. F. Chisholm, R. De Marco, J. Liu, S. Yang, S. P. Jiang, *ACS Appl. Energy Mater.* **2018**, *1*, 5286–5297.
[119] Y. Cheng, S. Zhao, B. Johannessen, J. P. Veder, M. Saunders, M. R. Rowles, M. Cheng, C. Liu, M. F. Chisholm, R. De Marco, H. M. Cheng, S. Z. Yang, S. P. Jiang, *Adv. Mater.* **2018**, *30*, e1706287.
[120] G. Vile, D. Albani, M. Nachtegaal, Z. Chen, D. Dontsova, M. Antonietti, N. Lopez, J. Perez-Ramirez, *Angew. Chem. Int. Ed.* **2015**, *54*, 11265-11269.
[121] G. Gao, Y. Jiao, E. R. Waclawik, A. Du, *J. Am. Chem. Soc.* **2016**, *138*, 6292-6297.
[122] J. A. Rodriguez-Manzo, M. Terrones, H. Terrones, H. W. Kroto, L. Sun, F. Banhart, *Nat. Nanotechnol.* **2007**, *2*, 307-311.
[123] Y. Cheng, S. He, S. Lu, J. P. Veder, B. Johannessen, L. Thomsen, M. Saunders, T. Becker, R. De Marco, Q. Li, S. Z. Yang, S. P. Jiang, *Adv. Sci.* **2019**, *6*, 1802066.
[124] P. Lu, Y. Yang, J. Yao, M. Wang, S. Dipazir, M. Yuan, J. Zhang, X. Wang, Z. Xie, G. Zhang, *Appl. Catal., B* **2019**, *241*, 113-119.

[125] C. Yan, H. Li, Y. Ye, H. Wu, F. Cai, R. Si, J. Xiao, S. Miao, S. Xie, F. Yang, Y. Li, G. Wang, X. Bao, *Energy Environ. Sci.* **2018**, *11*, 1204-1210.
[126] J. Wu, H. Zhou, Q. Li, M. Chen, J. Wan, N. Zhang, L. Xiong, S. Li, B. Y. Xia, G. Feng, M. Liu, L. Huang, *Adv. Energy Mater.* **2019**, *9*, 1900149.
[127] M. Zhao, Y. Wang, Q. Ma, Y. Huang, X. Zhang, J. Ping, Z. Zhang, Q. Lu, Y. Yu, H. Xu, Y. Zhao, H. Zhang, *Adv. Mater.* **2015**, *27*, 7372-7378.
[128] X. Liu, Z. Yan, Y. Zhang, Z. Liu, Y. Sun, J. Ren, X. Qu, *ACS Nano* **2019**, *13*, 5222-5230.
[129] H. Zhang, J. Wei, J. Dong, G. Liu, L. Shi, P. An, G. Zhao, J. Kong, X. Wang, X. Meng, J. Zhang, J. Ye, *Angew. Chem. Int. Ed.* **2016**, *55*, 14310-14314.
[130] Z. Liang, C. Qu, D. Xia, R. Zou, Q. Xu, *Angew. Chem. Int. Ed.* **2018**, *57*, 9604-9633.
[131] T. He, S. Chen, B. Ni, Y. Gong, Z. Wu, L. Song, L. Gu, W. Hu, X. Wang, *Angew. Chem. Int. Ed.* **2018**, *57*, 3493-3498.
[132] A. M. Abdel-Mageed, B. Rungtaweevoranit, M. Parlinska-Wojtan, X. Pei, O. M. Yaghi, R. J. Behm, *J. Am. Chem. Soc.* **2019**, *141*, 5201-5210.
[133] D. Wu, F. Xu, B. Sun, R. Fu, H. He, K. Matyjaszewski, *Chem. Rev.* **2012**, *112*, 3959-4015.
[134] P. Gélin, M. Primet, *Appl. Catal., B* **2002**, *39*, 1-37.
[135] D. Sellmann, D. Häußinger, F. W. Heinemann, *Eur. J. Inorg. Chem.* **1999**, *1999*, 1715-1725.
[136] P. Hou, H. Orikasa, H. Itoi, H. Nishihara, T. Kyotani, *Carbon* **2007**, *45*, 2011-2016.
[137] L. Wang, M. X. Chen, Q. Q. Yan, S. L. Xu, S. Q. Chu, P. Chen, Y. Lin, H. W. Liang, *Sci. Adv.* **2019**, *5*, eaax6322.
[138] S. Sun, G. Zhang, N. Gauquelin, N. Chen, J. Zhou, S. Yang, W. Chen, X. Meng, D. Geng, M. N. Banis, R. Li, S. Ye, S. Knights, G. A. Botton, T.-K. Sham, X. Sun, *Sci. Rep.* **2013**, *3*, 3767–3775.
[139] C. Gao, S. Chen, Y. Wang, J. Wang, X. Zheng, J. Zhu, L. Song, W. Zhang, Y. Xiong, *Adv. Mater.* **2018**, *30*, e1704624.
[140] C. Zhang, J. Sha, H. Fei, M. Liu, S. Yazdi, J. Zhang, Q. Zhong, X. Zou, N. Zhao, H. Yu, Z. Jiang, E. Ringe, B. I. Yakobson, J. Dong, D. Chen, J. M. Tour, *ACS Nano* **2017**, *11*, 6930-6941.
[141] J. Kim, C. Roh, S. K. Sahoo, S. Yang, J. Bae, J. W. Han, H. Lee, *Adv. Energy Mater.* **2018**, *8*, 1701476.
[142] Z. Wang, S. M. Xu, Y. Xu, L. Tan, X. Wang, Y. Zhao, H. Duan, Y. F. Song, *Chem. Sci.* **2019**, *10*, 378-384.
[143] M. Babucci, F. E. Sarac Oztuna, L. M. Debefve, A. Boubnov, S. R. Bare, B. C. Gates, U. Unal, A. Uzun, *ACS Catal.* **2019**, *9*, 9905-9913.
[144] A. Uzun, V. Ortalan, N. D. Browning, B. C. Gates, *Chem. Commun.* **2009**, 4657-4659.
[145] Z. Kou, W. Zang, P. Wang, X. Li, J. Wang, *Nanoscale Horiz.* **2020**, *5*, 757-764.
[146] H. Zhou, T. Liu, X. Zhao, Y. Zhao, H. Lv, S. Fang, X. Wang, F. Zhou, Q. Xu, J. Xu, C. Xiong, Z. Xue, K. Wang, W. C. Cheong, W. Xi, L. Gu, T. Yao, S. Wei, X. Hong, J. Luo, Y. Li, Y. Wu, *Angew. Chem. Int. Ed.* **2019**, *58*, 18388-18393.
[147] R. Lang, W. Xi, J. C. Liu, Y. T. Cui, T. Li, A. F. Lee, F. Chen, Y. Chen, L. Li, L. Li, J. Lin, S. Miao, X. Liu, A. Q. Wang, X. Wang, J. Luo, B. Qiao, J. Li, T. Zhang, *Nat. Commun.* **2019**, *10*, 234.
[148] T. W. Hansen, A. T. Delariva, S. R. Challa, A. K. Datye, *Acc. Chem. Res.* **2013**, *46*, 1720-1730.
[149] E. D. Boyes, P. L. Gai, *Ultramicroscopy* **1997**, *67*, 219-232.
[150] P. L. Gai, L. Lari, M. R. Ward, E. D. Boyes, *Chem. Phys. Lett.* **2014**, *592*, 355-359.
[151] S. Wei, A. Li, J. C. Liu, Z. Li, W. Chen, Y. Gong, Q. Zhang, W. C. Cheong, Y. Wang, L. Zheng, H. Xiao, C. Chen, D. Wang, Q. Peng, L. Gu, X. Han, J. Li, Y. Li, *Nat. Nanotechnol.* **2018**, *13*, 856-861.
[152] K. P. de Jong, A. J. Koster, *ChemPhysChem* **2002**, *3*, 776-780.
[153] O. Ersen, C. Hirlimann, M. Drillon, J. Werckmann, F. Tihay, C. Pham-Huu, C. Crucifix, P. Schultz, *Solid State Sci.* **2007**, *9*, 1088-1098.
[154] V. Ortalan, A. Uzun, B. C. Gates, N. D. Browning, *Nat. Nanotechnol.* **2010**, *5*, 506-510.
[155] L. Liu, N. Wang, C. Zhu, X. Liu, Y. Zhu, P. Guo, L. Alfilfil, X. Dong, D. Zhang, Y. Han, *Angew. Chem. Int. Ed.* **2020**, *59*, 819-825.

[156] K. Cao, T. Zoberbier, J. Biskupek, A. Botos, R. L. McSweeney, A. Kurtoglu, C. T. Stoppiello, A. V. Markevich, E. Besley, T. W. Chamberlain, U. Kaiser, A. N. Khlobystov, *Nat. Commun.* **2018**, *9*, 3382.
[157] X. C. Ren, X. Q. Zhang, R. Xu, J. Q. Huang, Q. Zhang, *Adv. Mater.* **2020**, *32*, e1908293.
[158] R. J. Celotta, S. B. Balakirsky, A. P. Fein, F. M. Hess, G. M. Rutter, J. A. Stroscio, *Rev. Sci. Instrum.* **2014**, *85*, 121301.
[159] J. A. Stroscio, R. J. Celotta, *Science* **2004**, *306*, 242-247.
[160] J. A. Stroscio, F. Tavazza, J. N. Crain, R. J. Celotta, A. M. Chaka, *Science* **2006**, *313*, 948-951.
[161] X. Sun, S. R. Dawson, T. E. Parmentier, G. Malta, T. E. Davies, Q. He, L. Lu, D. J. Morgan, N. Carthey, P. Johnston, S. A. Kondrat, S. J. Freakley, C. J. Kiely, G. J. Hutchings, *Nat. Chem.* **2020**, *12*, 560–567.
[162] L. Cao, Q. Luo, J. Chen, L. Wang, Y. Lin, H. Wang, X. Liu, X. Shen, W. Zhang, W. Liu, Z. Qi, Z. Jiang, J. Yang, T. Yao, *Nat. Commun.* **2019**, *10*, 4849.
[163] J. Gu, C. S. Hsu, L. Bai, H. M. Chen, X. Hu, *Science* **2019**, *364*, 1091-1094.
[164] P. Li, M. Wang, X. Duan, L. Zheng, X. Cheng, Y. Zhang, Y. Kuang, Y. Li, Q. Ma, Z. Feng, W. Liu, X. Sun, *Nat. Commun.* **2019**, *10*, 1711.
[165] P. Serna, B. C. Gates, *J. Am. Chem. Soc.* **2011**, *133*, 4714-4717.
[166] X. Cui, K. Junge, X. Dai, C. Kreyenschulte, M. M. Pohl, S. Wohlrab, F. Shi, A. Bruckner, M. Beller, *ACS Cent. Sci.* **2017**, *3*, 580-585.
[167] C. Dessal, T. Len, F. Morfin, J.-L. Rousset, M. Aouine, P. Afanasiev, L. Piccolo, *ACS Catal.* **2019**, *9*, 5752-5759.
[168] S. Cao, Y. Zhao, S. Lee, S. Yang, J. Liu, G. Giannakakis, M. Li, M. Ouyang, D. Wang, E. C. H. Sykes, M. Flytzani-Stephanopoulos, *Sci. Adv.* **2020**, *6*, eaba3809.
[169] Y. Zhou, D. E. Doronkin, M. Chen, S. Wei, J.-D. Grunwaldt, *ACS Catal.* **2016**, *6*, 7799-7809.
[170] J. Singh, J. A. van Bokhoven, *Catal. Today* **2010**, *155*, 199-205.
[171] J. Li, Y. Tang, Y. Ma, Z. Zhang, F. F. Tao, Y. Qu, *ACS Appl Mater Interfaces* **2018**, *10*, 38134-38140.
[172] A. M. Abdel-Mageed, G. Kučerová, J. Bansmann, R. J. Behm, *ACS Catal.* **2017**, *7*, 6471-6484.
[173] J. M. Dreimann, E. Kohls, H. F. W. Warmeling, M. Stein, L. F. Guo, M. Garland, T. N. Dinh, A. J. Vorholt, *ACS Catal.* **2019**, *9*, 4308-4319.
[174] J. X. Liang, J. Lin, J. Liu, X. Wang, T. Zhang, J. Li, *Angew. Chem. Int. Ed.* **2020**, *132*, 12968-12975.
[175] G. Sun, Z. J. Zhao, R. Mu, S. Zha, L. Li, S. Chen, K. Zang, J. Luo, Z. Li, S. C. Purdy, A. J. Kropf, J. T. Miller, L. Zeng, J. Gong, *Nat. Commun.* **2018**, *9*, 4454.
[176] A. Kaftan, M. Kusche, M. Laurin, P. Wasserscheid, J. Libuda, *Appl. Catal., B* **2017**, *201*, 169-181.
[177] P. Panagiotopoulou, D. I. Kondarides, *J. Catal.* **2009**, *267*, 57-66.
[178] J. H. Pazmiño, M. Shekhar, W. Damion Williams, M. Cem Akatay, J. T. Miller, W. Nicholas Delgass, F. H. Ribeiro, *J. Catal.* **2012**, *286*, 279-286.
[179] X. Zhu, M. Shen, L. L. Lobban, R. G. Mallinson, *J. Catal.* **2011**, *278*, 123-132.
[180] W. Z. Yu, W. W. Wang, S. Q. Li, X. P. Fu, X. Wang, K. Wu, R. Si, C. Ma, C. J. Jia, C. H. Yan, *J. Am. Chem. Soc.* **2019**, *141*, 17548-17557.
[181] J. Li, L. Zhang, K. Doyle‐Davis, R. Li, X. Sun, *Carbon Energy* **2020**, 1-33.
[182] M. Favaro, W. S. Drisdell, M. A. Marcus, J. M. Gregoire, E. J. Crumlin, J. A. Haber, J. Yano, *ACS Catal.* **2017**, *7*, 1248-1258.
[183] J. P. Simonovis, A. Hunt, R. M. Palomino, S. D. Senanayake, I. Waluyo, *J. Phys. Chem. C* **2018**, *122*, 4488-4495.
[184] H. C. Kwon, M. Kim, J. P. Grote, S. J. Cho, M. W. Chung, H. Kim, D. H. Won, A. R. Zeradjanin, K. J. J. Mayrhofer, M. Choi, H. Kim, C. H. Choi, *J. Am. Chem. Soc.* **2018**, *140*, 16198-16205.
[185] X. Cui, H. Li, Y. Wang, Y. Hu, L. Hua, H. Li, X. Han, Q. Liu, F. Yang, L. He, X. Chen, Q. Li, J. Xiao, D. Deng, X. Bao, *Chem* **2018**, *4*, 1902-1910.
[186] Y. Tang, Y. Wang, J. Li, *J. Phys. Chem. C* **2017**, *121*, 11281-11289.

[187] Y. X. Zhao, Z. Y. Li, Z. Yuan, X. N. Li, S. G. He, *Angew. Chem. Int. Ed.* **2014**, *53*, 9482-9486.
[188] H. Wang, J. Liu, L. F. Allard, S. Lee, J. Liu, H. Li, J. Wang, J. Wang, S. H. Oh, W. Li, M. Flytzani-Stephanopoulos, M. Shen, B. R. Goldsmith, M. Yang, *Nat. Commun.* **2019**, *10*, 1–12.
[189] Y. Zhao, K. R. Yang, Z. Wang, X. Yan, S. Cao, Y. Ye, Q. Dong, X. Zhang, J. E. Thorne, L. Jin, K. L. Materna, A. Trimpalis, H. Bai, S. C. Fakra, X. Zhong, P. Wang, X. Pan, J. Guo, M. Flytzani-Stephanopoulos, G. W. Brudvig, V. S. Batista, D. Wang, *Proc. Natl. Acad. Sci. U. S. A.* **2018**, *115*, 2902-2907.
[190] H. Yan, Y. Lin, H. Wu, W. Zhang, Z. Sun, H. Cheng, W. Liu, C. Wang, J. Li, X. Huang, T. Yao, J. Yang, S. Wei, J. Lu, *Nat. Commun.* **2017**, *8*, 1070.
[191] J. Zhang, Y. Zhao, C. Chen, Y. C. Huang, C. L. Dong, C. J. Chen, R. S. Liu, C. Wang, K. Yan, Y. Li, G. Wang, *J. Am. Chem. Soc.* **2019**, *141*, 20118-20126.
[192] L. Belmonte, D. Rossetto, M. Forlin, S. Scintilla, C. Bonfio, S. S. Mansy, *Phys. Chem. Chem. Phys.* **2016**, *18*, 20104-20108.
[193] W. Liu, L. Zhang, X. Liu, X. Liu, X. Yang, S. Miao, W. Wang, A. Wang, T. Zhang, *J. Am. Chem. Soc.* **2017**, *139*, 10790-10798.
[194] Y. N. Gong, L. Jiao, Y. Qian, C. Y. Pan, L. Zheng, X. Cai, B. Liu, S. H. Yu, H. L. Jiang, *Angew. Chem. Int. Ed.* **2020**, *59*, 2705-2709.
[195] X. Wang, Z. Chen, X. Zhao, T. Yao, W. Chen, R. You, C. Zhao, G. Wu, J. Wang, W. Huang, J. Yang, X. Hong, S. Wei, Y. Wu, Y. Li, *Angew. Chem. Int. Ed.* **2018**, *57*, 1944-1948.
[196] W. Zang, T. Yang, H. Zou, S. Xi, H. Zhang, X. Liu, Z. Kou, Y. Du, Y. P. Feng, L. Shen, L. Duan, J. Wang, S. J. Pennycook, *ACS Catal.* **2019**, *9*, 10166-10173.
[197] C. Ling, Y. Ouyang, Q. Li, X. Bai, X. Mao, A. Du, J. Wang, *Small Methods* **2018**, *3*, 1800376.
[198] D. Wang, C. Ao, X. Liu, S. Fang, Y. Lin, W. Liu, W. Zhang, X. Zheng, L. Zhang, T. Yao, *ACS Appl. Energy Mater.* **2019**, *2*, 6497-6504.
[199] N. Maity, S. Barman, Y. Minenkov, S. Ould-Chikh, E. Abou-Hamad, T. Ma, Z. S. Qureshi, L. Cavallo, V. D'Elia, B. C. Gates, J.-M. Basset, *ACS Catal.* **2018**, *8*, 2715-2729.
[200] E. Díaz, A. Restrepo, F. Núñez-Zarur, *Organometallics* **2018**, *37*, 2023-2036.
[201] M. K. Samantaray, E. Pump, A. Bendjeriou-Sedjerari, V. D'Elia, J. D. A. Pelletier, M. Guidotti, R. Psaro, J. M. Basset, *Chem. Soc. Rev.* **2018**, *47*, 8403-8437.
[202] M. K. Samantaray, V. D'Elia, E. Pump, L. Falivene, M. Harb, S. Ould Chikh, L. Cavallo, J. M. Basset, *Chem. Rev.* **2020**, *120*, 734-813.
[203] J. R. Pankhurst, P. Iyengar, A. Loiudice, M. Mensi, R. Buonsanti, *Chem. Sci.* **2020**, *11*, 9296-9302.
[204] F. A. Pasha, A. Bendjeriou-Sedjerari, K.-W. Huang, J.-M. Basset, *Organometallics* **2014**, *33*, 3320-3327.
[205] F. A. Pasha, A. Bendjeriou-Sedjerari, E. Abou-Hamad, K. W. Huang, J. M. Basset, *Chem. Commun.* **2016**, *52*, 2577-2580.
[206] F. Le Quéméner, S. Barman, N. Merle, M. A. Aljuhani, M. K. Samantaray, Y. Saih, K. C. Szeto, A. De Mallmann, Y. Minenkov, K.-W. Huang, L. Cavallo, M. Taoufik, J.-M. Basset, *ACS Catal.* **2018**, *8*, 7549-7555.
[207] A. Bendjeriou-Sedjerari, J. M. Azzi, E. Abou-Hamad, D. H. Anjum, F. A. Pasha, K. W. Huang, L. Emsley, J. M. Basset, *J. Am. Chem. Soc.* **2013**, *135*, 17943-17951.
[208] B. Hamzaoui, J. D. Pelletier, E. Abou-Hamad, J. M. Basset, *Chem. Commun.* **2016**, *52*, 4617-4620.
[209] P. Avenier, M. Taoufik, A. Lesage, X. Solans-Monfort, A. Baudouin, A. de Mallmann, L. Veyre, J. M. Basset, O. Eisenstein, L. Emsley, E. A. Quadrelli, *Science* **2007**, *317*, 1056-1060.
[210] C. G. Williams, M. Wang, D. Skomski, C. D. Tempas, L. L. Kesmodel, S. L. Tait, *J. Phys. Chem. C* **2017**, *121*, 13183-13190.
[211] S. L. Tait, A. Langner, N. Lin, R. Chandrasekar, O. Fuhr, M. Ruben, K. Kern, *Chemphyschem* **2008**, *9*, 2495-2499.
[212] L. Chen, G. E. Sterbinsky, S. L. Tait, *J. Catal.* **2018**, *365*, 303-312.
[213] C. D. Tempas, T. W. Morris, D. L. Wisman, D. Le, N. U. Din, C. G. Williams, M. Wang, A. V. Polezhaev, T. S. Rahman, K. G. Caulton, S. L. Tait, *Chem. Sci.* **2018**, *9*, 1674-1685.

[214] M. Kosmulski, *Langmuir* **1997**, *13*, 6315-6320.
[215] L. Chen, I. S. Ali, G. E. Sterbinsky, J. T. L. Gamler, S. E. Skrabalak, S. L. Tait, *ChemCatChem* **2019**, *11*, 2843-2854.
[216] D. Skomski, C. D. Tempas, K. A. Smith, S. L. Tait, *J. Am. Chem. Soc.* **2014**, *136*, 9862-9865.
[217] L. Chen, I. S. Ali, S. L. Tait, *ChemCatChem* **2020**, *12*, 3576-3584.
[218] H. Schwarz, *Isr. J. Chem.* **2014**, *54*, 1413-1431.
[219] A. Zecchina, E. Groppo, *Proc. R. Soc. A* **2012**, *468*, 2087-2098.
[220] R. T. Hannagan, G. Giannakakis, M. Flytzani-Stephanopoulos, E. C. H. Sykes, *Chem. Rev.* **2020,** https://doi.org/10.1021/acs.chemrev.0c00078.
[221] G. Giannakakis, M. Flytzani-Stephanopoulos, E. C. H. Sykes, *Acc. Chem. Res.* **2019**, *52*, 237-247.
[222] S. Zhang, L. Nguyen, J. X. Liang, J. Shan, J. J. Liu, A. I. Frenkel, A. Patlolla, W. Huang, J. Li, F. F. Tao, *Nat. Commun.* **2015**, *6*, 7938.
[223] H. Zhang, T. Watanabe, M. Okumura, M. Haruta, N. Toshima, *Nat. Mater.* **2011**, *11*, 49-52.
[224] H. Zhang, L. Lu, K. Kawashima, M. Okumura, M. Haruta, N. Toshima, *Adv. Mater.* **2015**, *27*, 1383-1388.
[225] G. Kyriakou, M. B. Boucher, A. D. Jewell, E. A. Lewis, T. J. Lawton, A. E. Baber, H. L. Tierney, M. Flytzani-Stephanopoulos, E. C. Sykes, *Science* **2012**, *335*, 1209-1212.
[226] Z. Li, T. He, D. Matsumura, S. Miao, A. Wu, L. Liu, G. Wu, P. Chen, *ACS Catal.* **2017**, *7*, 6762-6769.
[227] J. Liu, F. R. Lucci, M. Yang, S. Lee, M. D. Marcinkowski, A. J. Therrien, C. T. Williams, E. C. Sykes, M. Flytzani-Stephanopoulos, *J. Am. Chem. Soc.* **2016**, *138*, 6396-6399.
[228] W. Lai, Z. Miao, Y. Wang, J. Wang, S. Chou, *Adv. Energy Mater.* **2019**, *9*, 1900722.
[229] S. J. Tauster, S. C. Fung, R. T. Baker, J. A. Horsley, *Science* **1981**, *211*, 1121-1125.
[230] M. Cargnello, V. V. Doan-Nguyen, T. R. Gordon, R. E. Diaz, E. A. Stach, R. J. Gorte, P. Fornasiero, C. B. Murray, *Science* **2013**, *341*, 771-773.
[231] P. Liu, Y. Zhao, R. Qin, L. Gu, P. Zhang, G. Fu, N. Zheng, *Sci. Bull.* **2018**, *63*, 675-682.
[232] Z. Xu, Y. Zhang, L. Qin, Q. Meng, Z. Xue, L. Qiu, G. Zhang, X. Guo, Q. Li, *Small* **2020**, e2002071.
[233] K. Tan, M. Dixit, J. Dean, G. Mpourmpakis, *Ind. Eng. Chem. Res.* **2019**, *58*, 20236-20246.
[234] Q. Chen, S. Li, Y. Liu, X. Zhang, Y. Tang, H. Chai, Y. Huang, *Sens. Actuators, B* **2020**, *305*, 127511–127519.
[235] D. Wang, H. Wu, S. Z. F. Phua, G. Yang, W. Qi Lim, L. Gu, C. Qian, H. Wang, Z. Guo, H. Chen, Y. Zhao, *Nat. Commun.* **2020**, *11*, 357.

Entry for the Table of Contents

REVIEW

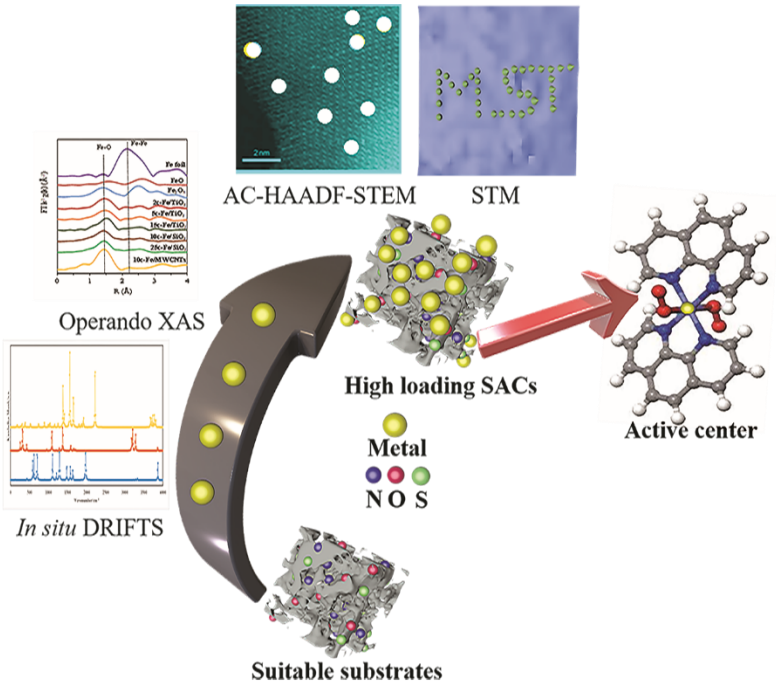

TOC description

This review provides an up-to-date comprehensive overview on fabrication of high metal loading single atom catalysts (SACs). *In situ* characterizations contribute greatly to the development of SACs. The well-defined structure of SACs also facilitates the analysis of the active center, guiding the design of catalysts from a trial-and-error practice into a reasonable design.

Biographies

Prof. Xinhua Liang joined the Department of Chemical and Biochemical Engineering at Missouri University of Science and Technology as an Assistant Professor in 2012 and was promoted to Associate Professor with tenure in 2017. He attended the Chemical Engineering program at Tianjin University, earning his B.S. in 2001 and M.S. in 2003. He received his Ph.D. in Chemical Engineering from the University of Colorado Boulder in 2008 and had three years' postdoctoral training there. Prof. Liang's research interests are in the areas of nanostructured materials preparation by atomic/molecular layer deposition (ALD/MLD), and their applications in various areas including catalysis and energy conversion and storage.

Kaiying Wang received his B.S. in chemical engineering from Beijing University of Chemical Technology, China. Now he is a PhD student at Missouri University of Science and Technology under the supervision of Prof. Xinhua Liang. His research focuses on nanostructured catalysts including single-atom catalysts for various reactions.

Prof. Xiaofeng Wang received his Ph.D. in chemical Engineering in 2018 from Missouri University of Science & Technology under the supervision of Prof. Xinhua Liang. Afterwards, he joined Dalian Maritime University, China as an Assistant Professor in the College of Environmental Science and Engineering. His recent research topics include catalytic conversion of biomass and environmental catalysis for air pollution control.